TABLE 3. Summary of Tumors with Acquired Resistance

ID	Gender	Histological Type	*EGFR* Mutation Status	Treatment	BOR	PFS	HGF	T790M	*MET* Amplification
KZ-1	M	Ad	Exon 19 del	Erlotinib	PR	254	60	−	+
KZ-2	F	Ad	L858R	Gefitinib	CR	1041	40	−	−
KZ-3	F	Ad	L858R	Gefitinib	PR	366	200	−	−
OK1—1	M	Ad	Exon 19 del	Gefitinib	PR	351	290	−	−
OK1—2							300	−	−
OK4—2	F	Ad	Exon 19 del	Gefitinib	PR	57	210	+	−
TS-1—3	F	Ad	L858R	Gefitinib	PR	180	90	−	−
TS-1—4							280	+	−
SG2	M	Ad	Exon 19 del	Gefitinib	PR	174	150	+	−
SG3	F	Ad	L858R	Gefitinib	SD	368	110	+	−
SG4	F	Ad	L858R	Gefitinib	PR	60	220	−	+
SG6	M	Ad	Exon 19 del	Gefitinib	PR	352	140	+	−
SG8	F	Ad	L858R	Gefitinib	SD	210	90	+	−
SG9	F	Ad	Exon 19 del	Gefitinib	SD	221	200	+	−
SG10	F	Ad	L858R	Gefitinib	CR	210	210	−	−
TB1—2	M	Ad	Exon 19 del	Gefitinib	PR	1770	230	+	−
TB2—2	F	AdSq	Exon 19 del	Gefitinib	PR	300	300	−	−
AC29—1	M	Ad	L858R	Gefitinib	PR	533	250	−	−
AC29—2							270	+	−
AC24	F	Ad	Exon 19 del	Gefitinib	PR	98	170	+	−
AC26	F	Ad	Exon 19 del	Gefitinib	SD	448	180	+	−
AC28	F	Ad	Exon 19 del	Gefitinib	PR	357	200	+	−
AC31	F	Ad	L858R	Gefitinib	PR	894	200	−	−

Ad, adeno; AdSq, adenosquamous; BOR, best overall response.

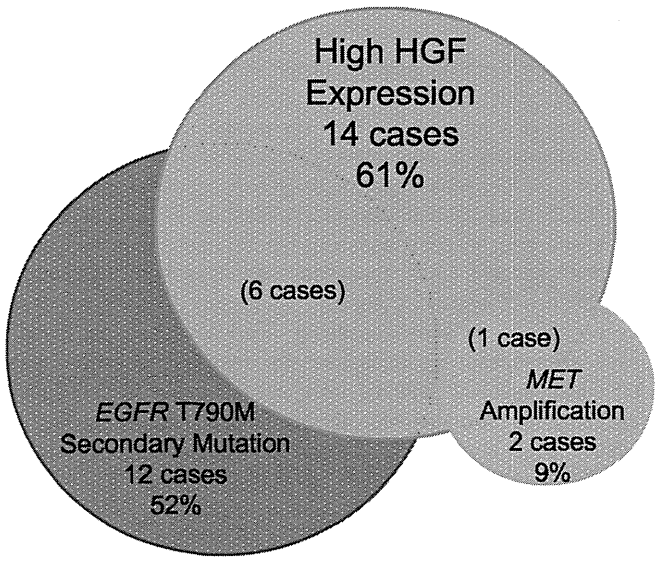

FIGURE 1. Incidences of high-level HGF expression, T790M secondary mutation, and *MET* amplification in 23 tumors with acquired resistance. Values in parentheses are the numbers of cases in which the tumors expressed two resistance factors simultaneously.

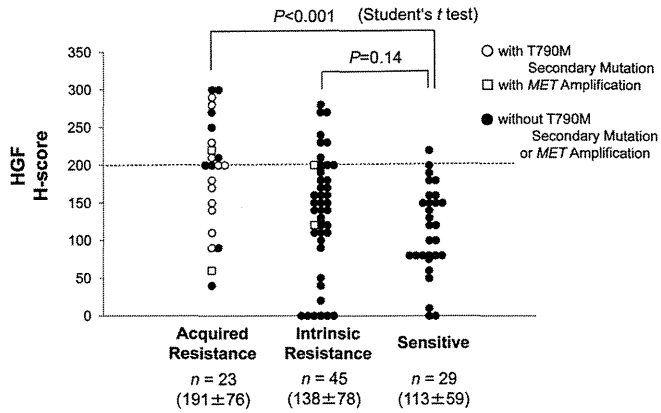

FIGURE 2. HGF expression score (*H* score) in EGFR-TKI-resistant tumors obtained from *EGFR* mutant lung cancer patients. Values in parentheses are mean ± SD of *H* score.

resistant tumors would be an ideal therapeutic target regardless of its origin.

It was of interest that a high level of HGF expression was detected in a small population of sensitive tumors. This was consistent with a previous report[16] indicating high-level HGF expression (*H* score ≥200) in several specimens from responders. Although the reason for the high level of HGF expression in tumors from responders is unclear at present, there are several possible explanations as follows. First, although HGF was expressed at high levels, natural inhibitors such as cleaved HGF and truncated MET, both of which inhibit binding of HGF to MET, may be generated in the tumors.[28,29] Second, negative regulators of MET tyrosine kinase activity such as protein kinase C may be activated and negate the effect of HGF on induction of EGFR-TKI resis-

tance in these tumors.[30] As the amounts of each clinical specimen were limited, we would like to perform further analyses in future studies should sufficient amounts of specimens become available.

Recent studies indicated that multiple resistance factors can be induced simultaneously in a single cancer. For example, Qi et al.[31] reported the simultaneous occurrence of *Met* mutation and activation of the EGFR pathway by ligand overexpression, similar to T790M mutation and HGF overexpression in EGFR mutant lung cancer, which caused resistance to Met-TKIs in gastric cancer. Katayama et al.[32] also reported that *ALK* gene amplification and gatekeeper mutation in *ALK* occurred simultaneously and conferred resistance to ALK inhibitors in EML4-ALK lung cancer. In this study, T790M secondary mutation and the high HGF expression level were simultaneously detected at high incidence (50%) in tumors with acquired resistance. Irreversible EGFR-TKIs were thought to have potential to control acquired resistance caused by T790M secondary mutation, but clinical responses were rarely observed in clinical trials.[33,34] We recently found that HGF induces resistance to not only reversible EGFR-TKIs but also irreversible EGFR-TKIs by activating the MET/PI3K/Akt pathway in *EGFR* mutant lung cancer cells with or without T790M secondary mutation.[26] Taken together, these observations suggest that HGF would be simultaneously expressed with T790M secondary mutation in tumors with acquired resistance and reduce the sensitivity to irreversible EGFR-TKIs in *EGFR* mutant lung cancer patients.

MET amplification has been detected in ~20% of tumors with acquired resistance to EGFR-TKIs in *EGFR* mutant lung cancer,[13,16,17] while the incidence reported in Japanese patients is rare.[14,18] Here, we detected *MET* amplification in two tumors (9%) with acquired resistance, suggesting that *MET* amplification can be detected in a significant proportion of tumors with acquired resistance even in Japanese patients. One case with high-level HGF expression and *MET* amplification (KZ-1) was treated with gefitinib and PFS was 254 days. The other case with low HGF and *MET* amplification (SG4) was treated with erlotinib and PFS was 60 days (Table 3). Although it is not possible to make definitive conclusions based on the data from only these two cases, the shorter PFS in the former case tentatively supports the observation that HGF accelerates expansion of preexisting clones with MET amplification.[16] Notably, simultaneous expression of these two factors was also detected in one tumor with intrinsic resistance (nonresponder). However, the mechanism by which HGF is induced in *EGFR* mutant lung cancer is still not well defined. Further examinations are warranted to elucidate the interaction between HGF expression and *MET* amplification in *EGFR* mutant lung cancer.

Among 68 resistant tumors, high-level HGF expression, T790M secondary mutation, and *MET* amplification were not detected in one tumor with acquired resistance and 31 tumors with intrinsic resistance, indicating the involvement of other mechanisms of resistance in these tumors. *EGFR* D761Y secondary mutation in exon 20 was detected in two tumors from the same patient.[24] *EGFR* D761Y mutation was originally identified in recurrent brain metastasis and was shown to induce intermediate-grade resistance to EGFR-TKIs.[35] In addition, rare secondary mutations (other than T790M and D761Y) or a preexisting resistance mutation in a minority of clones may also be involved in intrinsic resistance. Moreover, it was recently reported that a subpopulation of cancer cells that transiently exhibit a distinct phenotype characterized by engagement of IGF-1R activity, hypersensitivity to HDAC inhibition, and altered chromatin showed an intrinsic ability to tolerate exposure to EGFR-TKI.[36] Minor secondary mutations, a preexisting resistance mutation in a minority of clones, or chromatin-mediated drug resistance mechanisms may be involved in resistant tumors without high HGF expression, T790M secondary mutation, and *MET* amplification.

To overcome the HGF-induced resistance to EGFR-TKI in *EGFR* mutant lung cancer, double blockade of the EGFR pathway and HGF-MET pathway is therefore theoretically necessary.[14,16,27] To inhibit mutant EGFR with or without T790M secondary mutation, EGFR mutant-specific inhibitors were developed in addition to irreversible EGFR-TKIs.[37] To inhibit HGF-MET signaling, several inhibitors, including anti-HGF antibody, NK4 (natural antagonist of MET), and MET-TKIs, were developed.[16,25–27] Further studies are essential to determine optimal combined therapy with best efficacy and safety. In addition, a prospective study is required to determine whether immunohistochemical detection of HGF would be sufficiently reliable to identify patients with HGF-induced resistance to EGFR-TKIs. As levels of HGF in peripheral blood are correlated with clinical outcome to EGFR-TKIs in patients with non-small cell lung cancer,[38,39] such noninvasive methods may facilitate individual therapy for overcoming HGF-induced resistance to EGFR-TKIs in *EGFR* mutant lung cancer patients.

Recent studies indicated at least three important roles of HGF in EGFR-TKI resistance in *EGFR* mutant lung cancer. First, HGF induces resistance to reversible EGFR-TKIs, gefitinib, and erlotinib, by restoring MET/Gab1/PI3K/Akt pathways.[14,16] Second, HGF accelerates expansion of preexisting *MET*-amplified cancer cells and facilitates MET amplification-mediated resistance during EGFR-TKI treatment.[16] Third, after acquiring resistance to reversible EGFR-TKIs, HGF induces resistance of lung cancer cells with T790M secondary mutation to irreversible EGFR-TKIs.[24] Here, we detected high-level HGF expression frequently in tumors with intrinsic and acquired resistance to EGFR-TKIs in *EGFR* mutant lung cancer in Japanese patients. These findings indicate the value of HGF as a therapeutic target for EGFR-TKI-resistant *EGFR* mutant lung cancer. Therefore, combined therapy with EGFR-TKIs and HGF-MET inhibitors in patients with HGF-induced resistance may improve the clinical outcome of *EGFR* mutant lung cancer.

ACKNOWLEDGMENTS

Supported in part by Grant-in-Aid for Cancer Research from the Ministry of Health, Labor, and Welfare (to M.N., 16-1) and from the Ministry of Education, Science, Sports, and Culture of Japan (to S.Y. 21390256, 22112010A01).

REFERENCES

1. Lynch TJ, Bell DW, Sordella R, et al. Activating mutations in the epidermal growth factor receptor underlying responsiveness of non-small-cell lung cancer to gefitinib. *N Engl J Med* 2004;350:2129–2139.
2. Paez JG, Jänne PA, Lee JC, et al. EGFR mutations in lung cancer: correlation with clinical response to gefitinib therapy. *Science* 2004;304: 1497–1500.
3. Pao W, Miller V, Zakowski M, et al. EGF receptor gene mutations are common in lung cancers from "never smokers" and are associated with sensitivity of tumors to gefitinib and erlotinib. *Proc Natl Acad Sci U S A* 2004;101:13306–13311.
4. Mitsudomi T, Yatabe Y. Mutations of the epidermal growth factor receptor gene and related genes as determinants of epidermal growth factor receptor tyrosine kinase inhibitors sensitivity in lung cancer. *Cancer Sci* 2007;98:1817–1824.
5. Calvo E, Baselga J. Ethnic differences in response to epidermal growth factor receptor tyrosine kinase inhibitors. *J Clin Oncol* 2006;24:2158–2163.
6. Mitsudomi T, Morita S, Yatabe Y, et al; West Japan Oncology Group. Gefitinib versus cisplatin plus docetaxel in patients with non-small-cell lung cancer harbouring mutations of the epidermal growth factor receptor (WJTOG3405): an open label, randomised phase 3 trial. *Lancet Oncol* 2010;11:121–128.
7. Maemondo M, Inoue A, Kobayashi K, et al. Gefitinib or chemotherapy for non-small-cell lung cancer with mutated EGFR. *N Engl J Med* 2010;362:2380–2388.
8. Mok TS, Wu YL, Thongprasert S, et al. Gefitinib or carboplatin-paclitaxel in pulmonary adenocarcinoma. *N Engl J Med* 2009;361:947–957.
9. Jackman D, Pao W, Riely GJ, et al. Clinical definition of acquired resistance to epidermal growth factor receptor tyrosine kinase inhibitors in non-small-cell lung cancer. *J Clin Oncol* 2010;28:357–360.
10. Herbst RS, Heymach JV, Lippman SM. Lung cancer. *N Engl J Med* 2008;359:1367–1380.
11. Kobayashi S, Boggon TJ, Dayaram T, et al. EGFR mutation and resistance of non-small-cell lung cancer to gefitinib. *N Engl J Med* 2005;352:786–792.
12. Pao W, Miller VA, Politi KA, et al. Acquired resistance of lung adenocarcinomas to gefitinib or erlotinib is associated with a second mutation in the EGFR kinase domain. *PLoS Med* 2005;2:e73.
13. Engelman JA, Zejnullahu K, Mitsudomi T, et al. MET amplification leads to gefitinib resistance in lung cancer by activating ERBB3 signaling. *Science* 2007;316:1039–1043.
14. Yano S, Wang W, Li Q, et al. Hepatocyte growth factor induces gefitinib resistance of lung adenocarcinoma cells with EGF receptor mutations. *Cancer Res* 2008;68:9479–9487.
15. Matsumoto K, Nakamura T, Sakai K, et al. Hepatocyte growth factor and Met in tumor biology and therapeutic approach with NK4. *Proteomics* 2008;8:3360–3370.
16. Turke AB, Zejnullahu K, Wu YL, et al. Preexistence and clonal selection of MET amplification in EGFR mutant NSCLC. *Cancer Cell* 2010;17: 77–88.
17. Bean J, Brennan C, Shih JY, et al. MET amplification occurs with or without T790M mutations in EGFR mutant lung tumors with acquired resistance to gefitinib or erlotinib. *Proc Natl Acad Sci U S A* 2007;104: 20932–20937.
18. Onitsuka T, Uramoto H, Nose N, et al. Acquired resistance to gefitinib: the contribution of mechanisms other than the T790M, MET, and HGF status. *Lung Cancer* 2010;68:198–203.
19. Kosaka T, Yatabe Y, Endoh H, et al. Analysis of epidermal growth factor receptor gene mutation in patients with non-small cell lung cancer and acquired resistance to gefitinib. *Clin Cancer Res* 2006;12:5764–5769.
20. Herbst RS, Sun Y, Eberhardt WE, et al. Vandetanib plus docetaxel versus docetaxel as second-line treatment for patients with advanced non-small-cell lung cancer (ZODIAC): a double-blind, randomised, phase 3 trial. *Lancet Oncol* 2010;11:619–626.
21. Yatabe Y, Hida T, Horio Y, et al. A rapid, sensitive assay to detect EGFR mutation in small biopsy specimens from lung cancer. *J Mol Diagn* 2006;8:335–341.
22. Cappuzzo F, Hirsch FR, Rossi E, et al. Epidermal growth factor receptor gene and protein and gefitinib sensitivity in non-smallcell lung cancer. *J Natl Cancer Inst* 2005;97:643–655.
23. Hirsch FR, Herbst RS, Olsen C, et al. Increased EGFR gene copy number detected by fluorescent in situ hybridization predicts outcome in non-small-cell lung cancer patients treated with cetuximab and chemotherapy. *J Clin Oncol* 2008;26:3351–3357.
24. Toyooka S, Date H, Uchida A, et al. The epidermal growth factor receptor D761Y mutation and effect of tyrosine kinase inhibitor. *Clin Cancer Res* 2007;13:3431. author reply: 3431–3432.
25. Wang W, Li Q, Yamada T, et al. Crosstalk to stromal fibroblasts induces resistance of lung cancer to EGFR tyrosine kinase inhibitors. *Clin Cancer Res* 2009;15:6630–6638.
26. Yamada T, Matsumoto K, Wang W, et al. Hepatocyte growth factor reduces susceptibility to an irreversible epidermal growth factor receptor inhibitor in EGFR-T790M mutant lung cancer. *Clin Cancer Res* 2010; 16:174–183.
27. Okamoto W, Okamoto I, Tanaka K, et al. TAK-701, a humanized monoclonal antibody to hepatocyte growth factor, reverses gefitinib resistance induced by tumor-derived HGF in non-small cell lung cancer with an EGFR mutation. *Mol Cancer Ther* 2010;9:2785–2792.
28. Date K, Matsumoto K, Kuba K, et al. Inhibition of tumor growth and invasion by a four-kringle antagonist (HGF/NK4) for hepatocyte growth factor. *Oncogene* 1998;17:3045–3054.
29. Prat M, Crepaldi T, Gandino L, et al. C-terminal truncated forms of Met, the hepatocyte growth factor receptor. *Mol Cell Biol* 1991;11:5954–5962.
30. Gandino L, Di Renzo MF, Giordano S, et al. A tyrosine protein kinase activated by bombesin in normal fibroblasts and small cell carcinomas. *Oncogene* 1990;5:721–725.
31. Qi J, McTigue MA, Rogers A, et al. Multiple mutations and bypass mechanisms can contribute to development of acquired resistance to MET inhibitors. *Cancer Res* 2011;71:1081–1091.
32. Katayama R, Khan TM, Benes C, et al. Therapeutic strategies to overcome crizotinib resistance in non-small cell lung cancers harboring the fusion oncogene EML4-ALK. *Proc Natl Acad Sci U S A* 2011;108: 7535–7540.
33. Sequist LV, Besse B, Lynch TJ, et al. Neratinib, an irreversible pan-ErbB receptor tyrosine kinase inhibitor: results of a phase II trial in patients with advanced non-small-cell lung cancer. *J Clin Oncol* 2010; 28:3076–3083.
34. Jänne PA, Schellens JH, Engelman JA, et al. Preliminary activity and safety results from a phase I clinical trial of PF-00299804, an irreversible pan-HER inhibitor, in patients (pts) with NSCLC. *J Clin Oncol* 2008; 26:S20(abstr 8027).
35. Balak MN, Gong Y, Riely GJ, et al. Novel D761Y and common secondary T790M mutations in epidermal growth factor receptor-mutant lung adenocarcinomas with acquired resistance to kinase inhibitors. *Clin Cancer Res* 2006;12:6494–6501.
36. Sharma SV, Lee DY, Li B, et al. A chromatin-mediated reversible drug-tolerant state in cancer cell subpopulations. *Cell* 2010;141:69–80.
37. Zhou W, Ercan D, Chen L, et al. Novel mutant-selective EGFR kinase inhibitors against EGFR T790M. *Nature* 2009;462:1070–1074.
38. Kasahara K, Arao T, Sakai K, et al. Impact of serum hepatocyte growth factor on treatment response to epidermal growth factor receptor tyrosine kinase inhibitors in patients with non-small cell lung adenocarcinoma. *Clin Cancer Res* 2010;16:4616–4624.
39. Tanaka H, Kimura T, Kudoh S, et al. Reaction of plasma hepatocyte growth factor levels in non-small cell lung cancer patients treated with EGFR-TKIs. *Int J Cancer.* 2011;129:1410–1416.

Cancer Science
The official journal of the Japanese Cancer Association

Genetically engineered humanized anti-ganglioside GM2 antibody against multiple organ metastasis produced by GM2-expressing small-cell lung cancer cells

Tadaaki Yamada,[1] Hideaki Bando,[1] Shinji Takeuchi,[1] Kenji Kita,[1] Qi Li,[1] Wei Wang,[1] Shiro Akinaga,[2] Yasuhiko Nishioka,[3] Saburo Sone[3] and Seiji Yano[1,4]

[1]Division of Medical Oncology, Cancer Research Institute, Kanazawa University, Ishikawa; [2]Kyowa Hakko Kirin, Tokyo; [3]Department of Respiratory Medicine and Rheumatology, Institute of Health Biosciences, University of Tokushima Graduate School, Tokushima, Japan

(Received May 11, 2011/Revised August 24, 2011/Accepted September 1, 2011/Accepted manuscript online September 5, 2011/Article first published online September 30, 2011)

Small-cell lung cancer (SCLC) grows rapidly and metastasizes to multiple organs. We examined the antimetastatic effects of the humanized anti-ganglioside GM2 (GM2) antibodies, BIW-8962 and KM8927, compared with the chimeric antibody KM966, in a SCID mouse model of multiple organ metastases induced by GM2-expressing SCLC cells. BIW-8962 and KM8927 induced higher antibody-dependent cellular cytotoxicity and complement-dependent cytotoxicity than KM966 against the GM2-expressing SCLC cell line SBC-3 *in vitro*. These humanized antibodies inhibited the production of multiple organ metastases, increased the number of apoptotic cells, and prolonged the survival of the SCID mice. Histological analyses using clinical specimens showed that SCLC cells expressed GM2. These findings suggest that humanized anti-GM2 antibodies could be therapeutically useful for controlling multiple organ metastases of GM2-expressing SCLC. (*Cancer Sci* 2011; 102: 2157–2163)

Lung cancer is the leading cause of malignancy-related deaths worldwide.[1–3] Its high mortality rate has been attributed to its high metastatic potential to multiple organs, including the brain, liver, bones, and lymph nodes.[4,5] Metastasis to these organs frequently causes severe symptoms, such as pain, paresis, and dyspnea, and decreases patients' quality of life.[6] Approximately 15% of lung tumors are classified as small-cell lung cancer (SCLC); these tumors grow and metastasize to multiple organs much faster than non-small-cell lung cancer (NSCLC).[7] Although initially sensitive to conventional chemotherapy and radiotherapy, SCLC tumors eventually relapse and become refractory to conventional chemotherapy agents.[8] In addition, although several molecularly targeted drugs, such as the epidermal growth factor receptor (EGFR) tyrosine kinase inhibitors gefitinib and erlotinib and the angiogenesis inhibitor bevacizumab, are successful in the treatment of NSCLC, no effective molecularly targeted drugs are currently available for SCLC. Therefore, novel therapeutic methods are essential for improving the poor prognosis of patients with this disease.

Ganglioside GM2 (GM2) is a glycolipid that localizes to plasma membranes and is involved in cell adhesion and signal transduction. GM2 also plays crucial roles in metastasis.[9,10] Highly metastatic tumor cells contain higher amounts of gangliosides than do tumor cells with low metastatic potential.[11,12] Moreover, normal cells such as fibroblasts and epithelial cells express little GM2, indicating that GM2 is an ideal target for antimetastatic therapy.

We recently established a multiple organ metastasis model in natural killer (NK) cell-depleted SCID mice, consisting of the GM2-expressing SCLC cell line SBC-3. We found that the chimeric anti-GM2 antibody, KM966, induced antibody-dependent cellular cytotoxicity (ADCC) and inhibited multiple organ metastasis of SBC-3 cells *in vivo*.[13,14] Moreover, these SBC-3 cells continued to express GM2 even after becoming resistant to adriamycin.[15,16] These findings provide a therapeutic rationale for the use of anti-GM2 antibody in treating drug-resistant metastatic SCLC. Chimeric antibodies, however, may cause several adverse events, including infusion reactions and the generation of antibodies to these chimeric antibodies,[17–20] because the latter still contain mouse-derived protein sequences.

These problems have been solved by the development of humanized and fully human mAb.[21] Recently, several technologies have been used to further augment the therapeutic potential of humanized antibodies. For example, Potelligent technology (Kyowa Hakko Kirin, Tokyo, Japan) deletes fucose from the antibody, dramatically augmenting ADCC activity,[22] whereas Complegent technology (Kyowa Hakko Kirin, Tokyo, Japan) incorporates IgG3 sequences into IgG1 antibodies, thus augmenting complement-dependent cytotoxicity (CDC) activity. Using these technologies, we have generated two humanized anti-GM2 antibodies. BIW-8962 is a Potelligent antibody with high ADCC activity; KM8927 is a Potelligent and Complegent antibody generated from BIW-8962, with high ADCC and CDC activities. We have assessed the antimetastatic potential of these two humanized anti-GM2 antibodies against GM2-expressing SCLC cells, by evaluating their ADCC and CDC activities in the presence of human mononuclear cells (MNC) and human serum, respectively. We also examined the therapeutic potential of these antibodies in our SCLC multiple organ metastasis model, as well as assaying GM2 expression in clinical specimens obtained from SCLC patients.

Materials and Methods

Cell lines and culture conditions. The SBC-3 human SCLC cell line was the kind gift of Drs M. Tanimoto and K. Kiura (Okayama University, Okayama, Japan).[13] These cells were cultured in RPMI-1640 medium or DMEM, supplemented with 10% FBS, penicillin (100 U/mL), and streptomycin (50 μg/mL), in a humidified CO_2 incubator at 37°C.

Reagents. The anti-mouse interleukin-2 receptor β chain mAb, TM-β1 (IgG2b), was kindly supplied by Drs M. Miyasaka and T. Tanaka (Osaka University, Osaka, Japan).[23] KM966, a chimeric murine–human IgG1 mAb directed against GM2, and

[4]To whom all correspondence should be addressed.
E-mail: syano@staff.kanazawa-u.ac.jp

doi: 10.1111/j.1349-7006.2011.02093.x

BIW-8962 and KM8927, humanized anti-GM2 mAbs, were synthesized by Kyowa Hakko Kirin (Tokyo, Japan).

Flow cytometry. GM2 expression on SBC-3 cells was examined by flow cytometry.[24] Briefly, cells (5×10^5) were resuspended in PBS, supplemented with 10% pooled AB serum to prevent non-specific binding to the Fc receptor, washed with cold PBS and incubated on ice for 30 min with the humanized anti-GM2 mAb or control IgG. The cells were washed with cold PBS, incubated on ice for an additional 30 min with FITC-conjugated anti-human IgG antibody (Beckman Coulter, Fullerton, CA, USA), washed and resuspended in cold PBS. Cells were analyzed on a FACSCalibur flow cytometer with CellQuest software (Becton Dickinson, San Jose, CA, USA). The mean specific fluorescence intensity was calculated as the ratio of the mean fluorescence intensity of anti-GM2 mAb to that of control mAb.

***In vitro* effect of anti-GM2 antibody on proliferation of SBC-3 cells.** SBC-3 cells at 80% confluence were harvested, seeded at 2×10^3 cells per well in 96-well plates, and incubated in RPMI-1640 for 24 h. Anti-GM2 antibodies (BIW-8962, KM8927, or KM966) were added at various concentrations, and the cultures were incubated for 72 h at 37°C. A 50 μL aliquot of MTT solution (2 mg/mL; Sigma, St. Louis, MO, USA) was added to each well and the cells were incubated for 2 h at 37°C.[25] The media were removed and the dark blue crystals in each well were dissolved in 100 μL DMSO. Absorbance was measured with an MTP-120 microplate reader (Corona Electric, Ibaraki, Japan) at test and reference wavelengths of 550 nm and 630 nm, respectively. Data shown are representative of three independent experiments.

Isolation of human PBMC. Peripheral blood MNC were separated from heparinized venous blood samples drawn from healthy donors, diluted twofold with PBS in lymphocyte separation medium (Litton Bionetics, Kensington, MD, USA), and resuspended in medium for use in ADCC and CDC assays.

Antibody-dependent cellular cytotoxicity activity of anti-GM2 antibodies. SBC-3 cells at 80% confluence were harvested, seeded at 5×10^3 cells per well in 96-well plates, and incubated in the presence of human MNC cells (1×10^5 cells per well) and various concentrations of anti-GM2 antibody (BIW-8962, KM8927, or KM966) in RPMI-1640 for 4 h at 37°C. The ADCC activity was analyzed using the lactate dehydrogenase (LDH) releasing assay (LDH Cytotoxic Test; Wako, Osaka, Japan), in accordance with the manufacturer's protocols.

Complement-dependent cytotoxicity activity of anti-GM2 antibodies. SBC-3 cells at 80% confluence were harvested, seeded at 5×10^3 cells per well in 96-well plates, and incubated with diluted human serum (complement) and various concentrations of anti-GM2 antibody (BIW-8962, KM8927, or KM966) in RPMI-1640 for 4 h at 37°C. The CDC activity was assayed using the LDH Cytotoxic Test (Wako), in accordance with the manufacturer's protocols.

Purification of human peripheral lymphocytes and monocytes. Leukocytes were obtained from peripheral blood (200 mL) of healthy donors using an RS-6600 rotor of a Kubota KR-400 centrifuge, and PBMC were separated from granulocytes in lymphocyte separation medium (Organon Teknika, Durham, NC, USA). The PBMC were further separated into lymphocytes and monocytes by centrifugal elutriation in a Beckman JE-5.0 elutriation system (Beckman Instruments, Fullerton, CA, USA).[14] Fractions enriched in lymphocytes (>99%) and monocytes (>95%) were obtained at 2000*g* with flow rates of 26 and 30–36 mL/min, respectively. More than 97% of the cells were viable, as judged by the Trypan blue dye exclusion test. The monocyte fraction was washed twice with PBS and resuspended in RPMI-1640 medium supplemented with 5% FBS. At this point, >90% of the cells were monocytes, as judged by their morphology and non-specific esterase staining, and were used as monocytes for the experiments.

Animals. Male SCID mice, 5–6 weeks old, were obtained from Nihon Clea (Shizuoka, Japan) and maintained under specific pathogen-free conditions. All animal experiments complied with the Guidelines for the Institute for Experimental Animals, Kanazawa University Advanced Science Research Center (approval no. AP-081088).

SBC-3 cell model of multiple-organ metastasis and antimetastatic effect of anti-GM2 Ab. To facilitate the metastasis of SBC-3 cells, SCID mice were depleted of NK cells.[26] Briefly, 2 days before tumor cell inoculation, each mouse was injected i.p. with TM-β1 mAb (300 μg/300 μL PBS/mouse). Subconfluent SBC-3 cells were harvested and washed with Ca^{2+}-free and Mg^{2+}-free PBS. Cell viability was determined by the Trypan blue exclusion test, and only single cell suspensions of >90% viability were used. Cells (1×10^6/300 μL) were injected into the lateral tail vein of mice on day 0. To determine the optimum timing and dosage of anti-GM2 antibody, tumor-bearing mice were injected i.p. with control IgG (10 μg/100 μL) on days 7, 14, 21, 28, and 35, or with anti-GM2 antibody (0.1, 1, 10 μg/100 μL) on days 7, 14, 21, 28, and 35. Six weeks after tumor cell inoculation, the mice were anesthetized by i.p. injection of 0.5 mg pentobarbital and killed by cutting the subclavian artery. All major organs were removed, and the number of macroscopic metastatic lesions >0.5 mm in diameter in these organs was counted. Immunofluorescence with anti-NKp46 Ab showed that NK cells were depleted, at least, in the liver longer than 6 weeks (Fig. S1).

Detection of proliferating cells and apoptotic cells. *In vivo* cell proliferation was quantitated using mouse anti-human Ki-67 mAb (MIB1; Pharmingen, San Diego, CA, USA). Mouse livers were fixed in 10% formalin, followed by processing of 4-μm thick tissue sections. The sections were immersed in 0.01 M citrate buffer (pH 6.0) and boiled in a microwave oven for 10 min for antigen retrieval.

Apoptosis was quantitated in frozen tissue sections using the TdT-mediated TUNEL method, using an Apoptosis Detection System (Promega, Madison, WI, USA). Briefly, frozen tissue sections (9 μm thick) were fixed in PBS containing 4% formalin, washed with PBS and permeabilized with 0.2% Triton X-100. Following equilibration, nucleotide mix and terminal deoxynucleotidyl transferase were added, and DNA strand breaks were labeled with fluorescein-12-dUTP. The reactions were stopped by adding saline sodium citrate, and the localized green fluorescence of apoptotic cells was detected by fluorescence microscopy (×200). All sections were counterstained with H&E for routine histological examinations.

Detection of NK cells in liver metastasis. Frozen sections (4-μm thick) of liver metastasis produced by SBC-3 cells in NK cell-depleted SCID mice were fixed with cold acetone. After washing, sections were blocked with 5% FBS in PBS for 10 min, and incubated with 10 μg/mL anti-NKp46 Ab conjugated with FITC (1:100, for detecting NK cells; eBioscience, San Diego, CA, USA) at 4°C overnight. After washing with PBS, the section was counterstained using Vectashield with DAPI (Vector Laboratories, Burlingame, CA, USA). Fluorescence was detected by fluorescence microscopy (×400).

Detection of GM2 expression in tumors. Five clinical tumor specimens were obtained from five SCLC patients at Kanazawa University Hospital (Kanazawa, Japan). All five patients provided written informed consent, and the study protocol was approved by the Institutional Review Board of Kanazawa University Hospital. Liver metastasis produced by SBC-3 cells in NK cell-depleted SCID mice were also evaluated for GM2 expression. Frozen sections (4-μm thick) of these clinical and preclinical specimens were fixed with cold acetone. After washing, sections were blocked with 5% FBS in PBS for 10 min, and incubated with 10 μg/mL anti-GM2 Ab (BIW-8962) conjugated with Alexa Fluor488 (Invitrogen, Carlsbad, CA, USA) at 4°C

doi: 10.1111/j.1349-7006.2011.02093.x

overnight. After washing with PBS, sections were counterstained with Vectashield with DAPI (Vector Laboratories).

Quantification of immunohistochemistry and immunofluorescence. The five areas containing the highest numbers of stained cells within a section were selected for histologic quantitation by light or fluorescent microscopy under 200-fold magnification. All results were independently evaluated by two investigators (T.Y. and H.B.).

Statistical analysis. All data were expressed as the mean ± SD and were analyzed by one-way ANOVA using GraphPad Prism version 4.01 (GraphPad Software, San Diego, CA, USA). $P < 0.05$ was considered statistically significant.

Results

Effect of anti-GM2 antibody on GM2-expressing SBC-3 cells *in vitro*. Using FACS, we found that the SBC-3 SCLC cell line expressed large amounts of surface GM2 (Fig. 1A). Neither the humanized anti-GM2 antibodies, BIW-8962 and KM8927, nor the chimeric anti-GM2 antibody, KM966, affected the growth of SBC-3 cells *in vitro* (Fig. S2). In the presence of human MNC, all three anti-GM2 mAbs induced ADCC activity against SBC-3 cells, with the humanized mAbs BIW-8962 and KM8927 having greater ADCC activity than the chimeric KM966 mAb, especially at lower Ab concentrations (0.01–0.10 μg/mL) (Fig. 1B). This phenomenon was confirmed at various effector/target cell ratios (10, 20, and 40) (Fig. 1C). We further purified lymphocytes and monocytes from MNC, and evaluated their potential to induce ADCC. Lymphocytes were more potent than monocytes in our experimental conditions, but both lymphocytes and monocytes induced considerable ADCC activity mediated by KM8927 against SBC-3 cells (Fig. S3).

Moreover, all three mAbs showed CDC activity against SBC-3 cells in the presence of human serum from healthy donors, with KM8927 having greater CDC activity than KM966 at concentrations of 1 μg/mL.

Effect of anti-GM2 antibodies on multiple organ metastasis of SBC-3 cells in NK cell-depleted SCID mice. To determine the optimal dose of anti-GM2 antibody *in vivo*, we treated SBC-3 bearing NK cell-depleted SCID mice with various concentrations of KM8927. We found that KM8927 inhibited the production of metastases in the liver, kidneys, and lymph nodes in a dose-dependent manner (Table 1), with 10 μg/dose being the most efficient dose of KM8927.

We next examined the effect of the treatment schedule. We found that i.p. injections of 10 μg KM8927, on days 7, 14, and 21 after inoculation of SBC-3 cells, were all effective in inhibiting the number of multiple organ metastases (Table 2, set 1), although starting KM8927 on day 7 showed the greatest level of inhibition. When we compared the effects of i.p. injections of 10 μg KM8927, BIW-8962, and KM966, beginning on day 7, we found that all three markedly inhibited multiple organ metastases of SBC-3 cells (Table 2, set 2).

To determine the mode of action of these anti-GM2 antibodies, we histologically analyzed liver metastases treated with PBS (control) or anti-GM2 antibodies (Fig. 2A). We found that the numbers of Ki-67-positive proliferating cells did not differ significantly when metastatic lesions were treated with PBS, KM8927, BIW-8962, or KM966. In contrast, the number of TUNEL-positive apoptotic cells was much higher in lesions treated with the anti-GM2 mAbs than with control, although there was no difference among the three types of anti-GM2 antibodies (Fig. 2B). Conversely, the number of GM2-positive cells was much lower in lesions treated with anti-GM2 antibodies

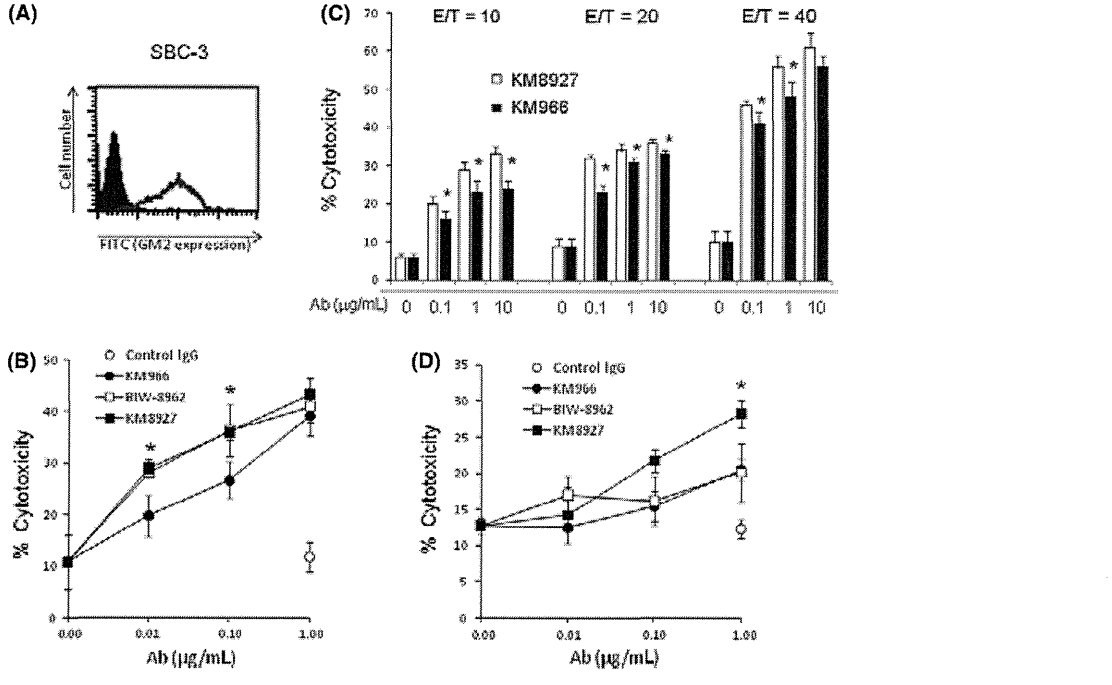

Fig. 1. Effect of anti-ganglioside GM2 antibody on GM2-expressing SBC-3 small-cell lung cancer cells *in vitro*. (A) Assay of GM2 expression on SBC-3 cells by flow cytometry. (B) Effects of three mAbs on antibody-dependent cellular cytotoxicity activity against SBC-3 cells in the presence of human mononuclear cells (MNC), as determined by 4-h LDH releasing assays. Effector (MNC)/target (SBC-3) ratio was 20. (C) Effects of various effector/target (E/T) ratios on antibody-dependent cellular cytotoxicity activity against SBC-3 cells in the presence of human MNC with KM8927 or KM966, as determined by 4-h LDH releasing assays. (D) Effects of three mAbs on complement-dependent cytotoxicity activity against SBC-3 cells in the presence of human serum, as determined by 4-h LDH releasing assays. Results shown are representative of at least three independent experiments. *$P < 0.05$ compared with KM966.

Table 1. Dose-dependent effect of KM8927 antibody against multiple organ metastasis by SBC-3 small-cell lung cancer cells in natural killer cell-depleted SCID mice

Treatment	Dose (μg)	Liver		Kidneys	
		No. of metastatic colonies	Incidence median (range)	No. of metastatic colonies	Incidence median (range)
Control		5/5	25 (8–45)	5/5	5 (3–7)
Control IgG		5/5	24 (8–45)	4/5	5 (0–8)
KM8927	0.1	5/5	20 (8–48)	4/5	3 (0–8)
	1.0	5/5	14 (4–39)	3/5	4 (0–9)
	10.0	3/5	7 (0–9)*	2/5	0 (0–2)*

SBC-3 (1×10^6) small-cell lung cancer cells were i.v. inoculated into SCID mice depleted of natural killer cells. For control and control IgG, PBS (100 μL) and human IgG (10 μg), respectively, were used. Treatment with KM8927 (0.1 μg, 1.0 μg, 10.0 μg), PBS, or human IgG, was given once a week on days 7, 14, 21, 28, and 35. The mice were killed and metastasis production was valuated. The data shown are representative of two independent experiments. *Significantly different from control group ($P < 0.05$).

Table 2. Effect of various anti-ganglioside GM2 antibodies against multiple organ metastasis by SBC-3 small-cell lung cancer cells in natural killer cell-depleted SCID mice

Treatment	Day of therapy	Liver		Kidneys		Lymph nodes	
		No. of metastatic colonies	Incidence median (range)	No. of metastatic colonies	Incidence median (range)	No. of metastatic colonies	Incidence median (range)
Set 1							
Control	7	5/5	6 (2–14)	2/5	1 (0–1)	5/5	7 (3–9)
KM8927	7	2/5	0 (0–1)*	0/5	0 (0–0)	3/5	1 (0–2)*
	14	5/5	2 (1–3)	2/5	0 (0–5)	4/5	1 (0–3)*
	21	4/5	2 (0–2)	4/5	1 (0–2)	4/5	3 (0–4)*
Set 2							
Control	7	5/5	24 (20–32)	5/5	5 (1–7)	5/5	10 (6–12)
Control IgG	7	5/5	15 (14–20)	5/5	3 (2–4)	5/5	6 (3–14)
KM966	7	5/5	7 (5–9)*	3/5	1 (0–3)*	4/5	2 (0–5)*
BIW-8962	7	5/5	6 (2–18)*	3/5	2 (0–2)*	2/5	0 (0–3)*
KM8927	7	5/5	9 (1–14)*	3/5	2 (0–2)*	3/5	1 (0–3)*

SBC-3 (1×10^6) cells were i.v. inoculated into SCID mice depleted of natural killer cells. Set 1: PBS for control or KM8927 (10 μg/dose), was given once a week on day 7, 14, or 21. Set 2: PBS or indicated anti-GM2 antibodies (10 μg/dose) given once a week from day 7. The mice were killed on day 42 and metastasis production was valuated. The data shown are representative of two independent experiments. *Significantly different from control group ($P < 0.05$).

than in control lesions. Moreover, the number of GM2-positive cells trended to be fewer in lesions treated with KM8927 and BIW-8962 than with KM966.

In addition, we carried out additional staining to rule out the possibility that decreased GM2 staining of anti-GM2 Ab-treated tumors was due to a masking effect by anti-GM2 Ab used for therapy *in vivo*. For this purpose, liver metastatic lesions of control and KM8927-treated mice were stained with secondary Ab (anti-human IgG conjugated with Alexa Fluor488) alone or KM8927 and secondary Ab. In the liver lesion of control mice, high GM2 expression was detected when stained with KM8927 and secondary Ab, but it was no detected when stained with secondary Ab alone (Fig. S4). These results indicate the activity and specificity of these Abs. Under these experimental conditions, in the liver lesions of KM8927-treated mice, GM2 expression was considerably lower when stained with KM8927 and secondary Ab (Fig. S4). Importantly, GM2 was not detected when stained with secondary Ab alone, indicating that KM8927 Ab injected for treatment *in vivo* did not mask GM2 antigen and disturbed GM2 staining in this experiment.

We also assessed the effect of these anti-GM2 mAbs on the survival of SBC-3-bearing mice. KM8927 and BIW-8962 were injected once per week, from day 7, until the mice became moribund. We found that treatment with these mAbs dramatically prolonged survival of the mice compared with control (Fig. 3).

GM2 expression in clinical specimens obtained from SCLC patients. We also examined GM2 expression in tumors from SCLC patients by immunofluorescence and immunohistochemistry. We were able to evaluate only five surgical specimens, four primary tumors and a brain metastasis (sample no.1), because SCLC is rarely resected surgically and GM2 can be detected only in frozen sections. GM2-positive SCLC cells were present in three specimens, primary tumors from two patients and a brain metastasis from another patient (Fig. 4).

Discussion

Several mAbs have been successfully introduced into clinical practice to treat cancer patients. For example, the chimeric anti-EGFR mAb cetuximab and the fully human anti-EGFR mAb antibody panitumumab have been approved for the treatment of patients with colorectal cancer. These two antibodies are thought to have similar antitumor activity, but the humanized panitumumab was reported to have better adverse event profiles than the chimeric cetuximab. For example, several patients who were intolerant of cetuximab have been treated with panitumumab without evidence of infusion reactions or allergic responses.[27] We have shown here that the humanized anti-GM2 antibodies BIW-8962 and KM8927 have high therapeutic activities, at least equivalent to that of the chimeric antibody KM966, in our multiple organ metastasis model. Therefore, these humanized anti-GM2 antibodies may retain their therapeutic effect, while being less toxic than the chimeric KM966 antibody. Importantly, we could detect GM2-expressing SCLC cells in clinical specimens.

doi: 10.1111/j.1349-7006.2011.02093.x

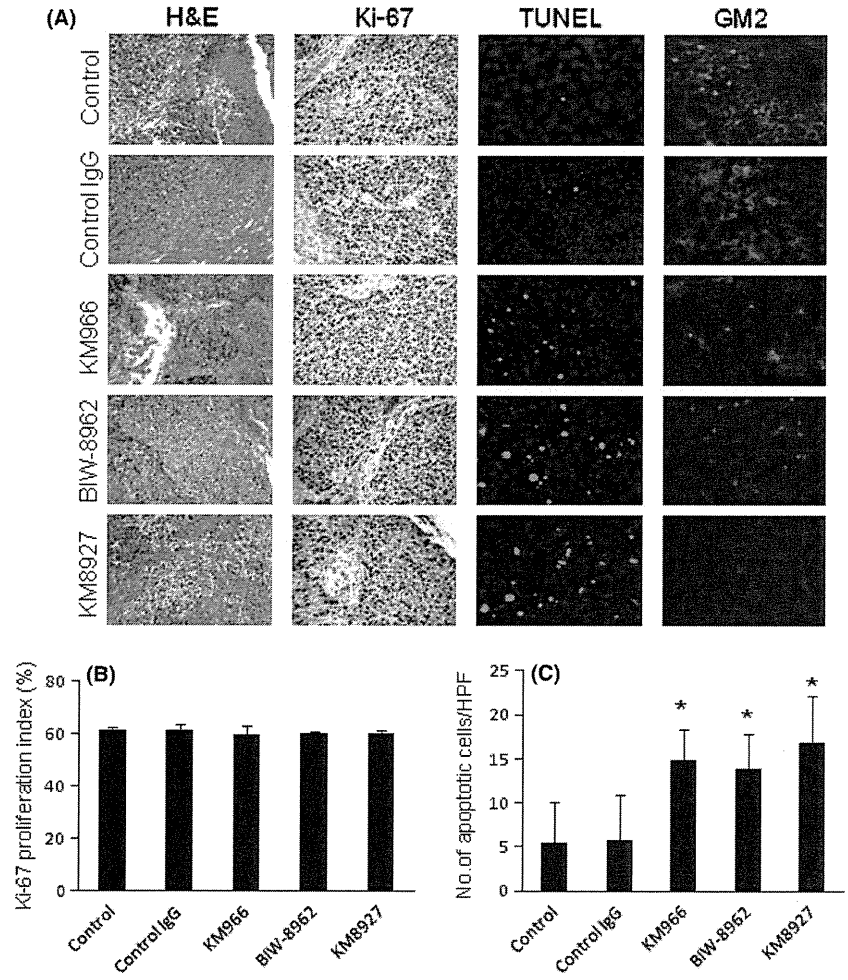

Fig. 2. Histological examination of metastatic lesions treated with anti-ganglioside GM2 antibodies. SBC-3 (1×10^6) small-cell lung cancer cells were inoculated i.v. into natural killer cell-depleted SCID mice. The mice were injected with PBS, control IgG, KM966, BIW-8962, or KM8927, on days 7, 14, 21, 28, and 35 and killed on day 42. Metastatic liver lesions were harvested and stained with H&E, and for Ki-67, an indicator of cell proliferation, TUNEL, an indicator of cell apoptosis, and GM2 expression. (A) Microscopic appearance of lesions. (B) Quantification of the percentage of Ki-67-positive cancer cells and (C) the number of TUNEL-positive apoptotic cells. Data shown are the mean ± SD of five independent areas. Results shown are representative of at least two independent experiments. HPF, high power field. *$P < 0.05$ compared with control.

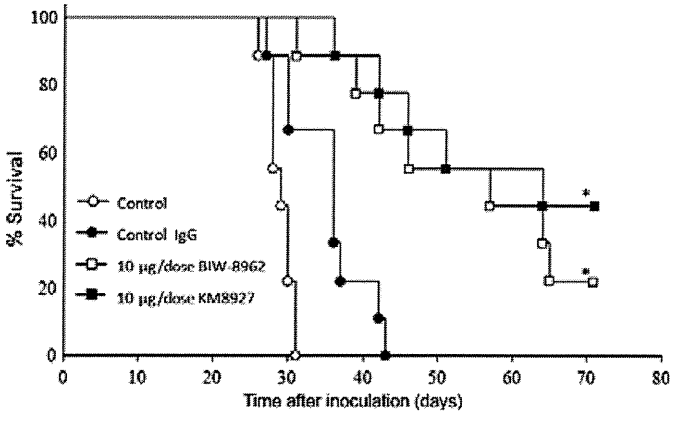

Fig. 3. Effect of anti-ganglioside GM2 antibodies on survival of SBC-3-bearing mice. SBC-3 (1×10^6) small-cell lung cancer cells were inoculated i.v. into natural killer cell-depleted SCID mice. The mice (10 per group) were treated with PBS, control IgG, KM966, BIW-8962, or KM8927, once a week starting on day 7. Results shown are representative of two independent experiments. *$P < 0.001$ compared with control.

These results collectively suggest a therapeutic rationale for the use of humanized anti-GM2 mAbs in patients with SCLC. In addition, spotty GM2 staining indicates that GM2 expression may be heterogenous among SCLC cells. Therefore, combined use of anti-GM2 Ab with other agents, such as cytotoxic chemotherapeutic drugs, might be necessary for controlling SCLC in patients.

Both ADCC and CDC are important activities of Ab therapy.[28] Potelligent technology was used to develop BIW-8962, with augmented ADCC activity, whereas both Potelligent and Complegent technologies were used to generate KM8927, with augmented ADCC and CDC activities. We found that BIW-8962 had higher ADCC activity using human MNC, and KM8927 had higher ADCC and CDC activities using human serum, than the chimeric anti-GM2 mAb KM966 *in vitro*. In contrast, the biological effects of these humanized anti-GM2 antibodies were similar to that of KM966 in our mouse metastasis model. This discrepancy may be due to differences in human and mouse biology. Generally, human and rabbit serum, but not mouse serum, has high CDC activity in the presence of antibody.[29] Moreover, although NK cells and monocytes/macrophages are the major effectors of ADCC using anti-GM2 antibody, mouse effector cells are much less potent than human

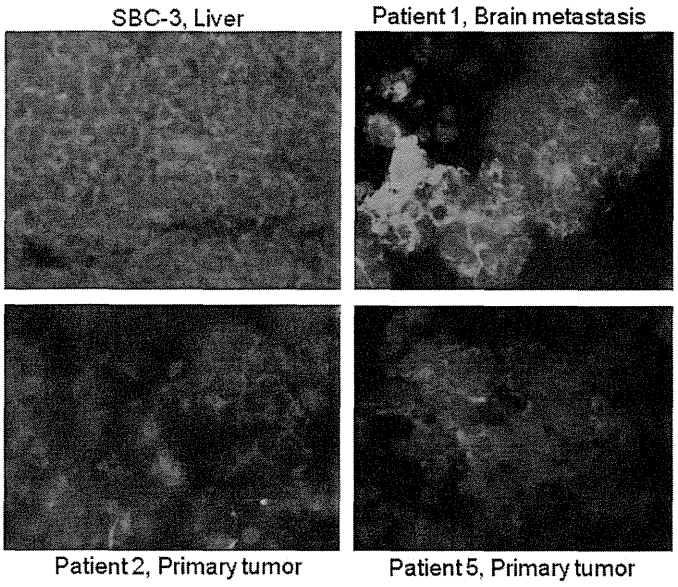

Fig. 4. Ganglioside GM2 expression in tumors obtained from patients with small-cell lung cancer. Clinical specimens obtained from the patients were assayed for GM2 expression by immunofluorescence and immunohistochemistry. Of five clinical specimens, three were positive for GM2; representative areas are shown. Results shown are representative of two independent stainings for each specimen.

effector cells in inducing ADCC.[14] We confirmed that human peripheral monocytes and lymphocytes induced considerable ADCC mediated by KM8927 against SBC-3 cells (Fig. S3). Furthermore, to facilitate the generation of multiple organ metastases, we depleted NK cells, the major effector cells, from SCID mice.[26] Thus, the humanized anti-GM2 antibodies generated by Potelligent and Complegent technologies may have greater therapeutic potential than chimeric KM966 in humans.

Prolongation of survival is the most reliable and clinically relevant endpoint of preclinical experiments. We found that injection of BIW-8962 and KM8927, beginning on day 7 after inoculation of SBC-3 cells, successfully prolonged the survival of SCID mice bearing multiple organ metastases of SBC-3 cells. In our model, i.v. inoculated SBC-3 cells produced micrometastases by day 7.[13] Small-cell lung cancer generates micrometastases in almost all patients, even when the primary tumor is still small in size. Therefore, these humanized anti-GM2 antibodies may at least prevent the enlargement of systemic micrometastases produced by GM2-expressing SCLC cells.

In conclusion, we have shown that the humanized anti-GM2 mAbs BIW-8962 and KM8927, generated by Potelligent and Complegent technologies, respectively, have therapeutic potential against multiple organ metastases of GM2-expressing SCLC cells. Clinical trials with BIW-8962 are now ongoing in previously treated multiple myeloma (NCT00775502).

Acknowledgments

We thank Drs. Katsuyuki Kiura and Mitsune Tanimoto (Okayama University) for kindly providing SBC-3 cells, and Dr. Masayuki Miyasaka (Osaka University) for providing the TM-β1 hybridoma. We also thank Ms Takako Sano (Kanazawa University), Mr. Takuya Kuramoto, and Yuko Oka (University of Tokushima) for expert technical assistance. This work was supported in part by Scientific Research on Innovative Areas "Integrative Research on Cancer Microenvironment Network" (S. Yano, 22112010A01) from the Ministry of Education, Culture, Sports, Science, and Technology of Japan.

Disclosure Statement

Seiji Yano received honoraria from Chugai Pharma and AstraZeneca. Seiji Yano received research fundings from Chugai Pharma and Kyowa Hakko Kirin. Shiro Akinaga is an employee of Kyowa Hakko Kirin.

References

1 Hoffman PC, Mauer AM, Vokes EE. Lung cancer. *Lancet* 2000; **355**: 479–85.
2 Quint LE, Francis IR, Wahl RL, Gross BH. *Imaging of Lung Cancer: Lung Cancer, Principles and Practice*. Philadelphia: Lippincott-Raven, 1996; 437–70.
3 Kenzaki K, Sakiyama S, Tomimoto H *et al.* Clinical analysis of elderly patients with primary lung cancer. *Kyobu Geka* 2010;**63**: 519–23; discussion 524–6.
4 Goya T, Asamura H, Yoshimura H *et al.* Prognosis of 6644 resected non-small cell lung cancers in Japan: a Japanese lung cancer registry study. *Lung Cancer* 2005; **50**: 227–34.
5 Mountain CF. A new international staging system for lung cancer. *Chest* 1986; **4**(Suppl): 225S–33S.
6 Yang P. Epidemiology of lung cancer prognosis: quantity and quality of life. *Methods Mol Biol* 2009; **471**: 469–86.
7 Mountain CF, Dresler CM. Regional lymph node classification for lung cancer staging. *Chest* 1997; **111**: 1718–23.
8 Sullivan FJ. *Palliative Radiotherapy for Lung Cancer: Lung Cancer, Principles and Practice*. Philadelphia: Lippincott-Raven, 1996; 775–89.
9 Portoukalian J, Zwingelstein G, Dore JF, Bourgoin JJ. Studies of a ganglioside fraction extracted from human malignant melanoma. *Biochimie* 1976; **58**: 1285–7.
10 Akasako Y, Nara K, Nagai Y, Hashimoto Y. Inhibition of ganglioside synthesis reduces the neuronal survival activity of astrocytes. *Neurosci Lett* 2011; **488**: 199–203.
11 Ravindranath MH, Tsuchida T, Morton DL, Irie RF. Ganglioside GM3:GD3 ratio as an index for the management of melanoma. *Cancer* 1991; **67**: 3029–35.
12 Laferte S, Fukuda MN, Fukuda M, Dell A, Dennis JW. Glycosphingolipids of lectin-resistant mutants of the highly metastatic mouse tumor cell line, MDAY-D2. *Cancer Res* 1987; **47**: 150–9.
13 Hanibuchi M, Yano S, Nishioka Y, Yanagawa H, Kawano T, Sone S. Therapeutic efficacy of mouse-human chimeric anti-ganglioside GM2 monoclonal antibody against multiple organ micrometastases of human lung cancer in NK cell-depleted SCID mice. *Int J Cancer* 1998; **78**: 480–5.
14 Hanibuchi M, Yano S, Nishioka Y, Yanagawa H, Sone S. Anti-ganglioside GM2 monoclonal antibody-dependent killing of human lung cancer cells by lymphocytes and monocytes. *Jpn J Cancer Res* 1996; **87**: 497–504.
15 Fukumoto H, Nishio K, Ohta S, Hanai N, Saijo N. Reversal of adriamycin resistance with chimeric anti-ganglioside GM2 antibody. *Int J Cancer* 1996; **67**: 676–80.
16 Hanibuchi M, Yano S, Nishioka Y, Yanagawa H, Miki T, Sone S. Immunological circumvention of multiple organ metastases of multidrug resistant human small cell lung cancer cells by mouse-human chimeric anti-ganglioside GM2 antibody KM966. *Clin Exp Metastasis* 2000; **18**: 353–60.
17 Langerak A, River G, Mitchell E, Cheema P, Shing M. Panitumumab monotherapy in patients with metastatic colorectal cancer and cetuximab infusion reactions: a series of four case reports. *Clin Colorectal Cancer* 2009; **8**: 49–54.
18 Heun J, Holen K. Treatment with panitumumab after a severe infusion reaction to cetuximab in a patient with metastatic colorectal cancer: a case report. *Clin Colorectal Cancer* 2007; **6**: 529–31.
19 Patel DD, Goldberg RM. Cetuximab-associated infusion reactions: pathology and management. *Oncology (Williston Park)* 2006; **20**:1373–82; discussion 1382, 1392–4, 1397.
20 Helbling D, Borner M. Successful challenge with the fully human EGFR antibody panitumumab following an infusion reaction with the chimeric EGFR antibody cetuximab. *Ann Oncol* 2007; **18**: 963–4.
21 Ura T. The current status of development of anti-EGFR antibodies. *Gan To Kagaku Ryoho* 2010; **37**: 777–81.
22 Shitara K. Potelligent antibodies as next generation therapeutic antibodies. *Yakugaku Zasshi* 2009; **129**: 3–9.
23 Tanaka T, Kitamura F, Nagasaka Y, Kuida K, Suwa H, Miyasaka M. Selective long-term elimination of natural killer cells in vivo by an anti-interleukin 2 receptor β chain monoclonal antibody in mice. *J Exp Med* 1993; **178**: 1103–7.

doi: 10.1111/j.1349-7006.2011.02093.x

24 Nishioka Y, Yano S, Fujiki F *et al.* Combined therapy of multidrug-resistant human lung cancer with anti-P-glycoprotein antibody and monocyte chemoattractant protein-1 gene transduction: the possibility of immunological overcoming of multidrug resistance. *Int J Cancer* 1997; **71**: 170–7.
25 Green LM, Reade JL, Ware CF. Rapid colorimetric assay for cell viability: application to the quantitation of cytotoxic and growth inhibitory lymphokines. *J Immunol Methods* 1984; **70**: 257–68.
26 Yano S, Nishioka Y, Izumi K *et al.* Novel metastasis model of human lung cancer in SCID mice depleted of NK cells. *Int J Cancer* 1996; **67**: 211–7.
27 Helbling D, Borner M. Successful challenge with the fully human EGFR antibody panitumumab following an infusion reaction with the chimeric EGFR antibody cetuximab. *Ann Oncol* 2007; **18**: 963–4.
28 Kubota T, Niwa R, Satoh M, Akinaga S, Shitara K, Hanai N. Engineered therapeutic antibodies with improved effector functions. *Cancer Sci* 2009; **100**: 1566–72.
29 Klehr M, Koehl U, Mühlenhoff M *et al.* The novel chimeric anti-NCAM (neural cell adhesion molecule) antibody ch.MK1 displays antitumor activity in SCID mice but does not activate complement-dependent cytolysis (CDC). *J Immunother* 2009; **32**: 442–51.

Supporting Information

Additional Supporting Information may be found in the online version of this article:

Fig. S1. Detection of natural killer cells and macrophages in liver metastasis.

Fig. S2. Effects of mAbs BIW-8962, KM8927, and KM966 on the growth of SBC-3 small-cell lung cancer cells, as determined by MTT assays.

Fig. S3. Effects of KM8927 on antibody-dependent cellular cytotoxicity activity against SBC-3 small-cell lung cancer cells in the presence of human lymphocytes and monocytes, as determined by 4-h LDH releasing assays.

Fig. S4. Ganglioside GM2 expression in liver lesions produced by small-cell lung cancer SBC-3 cells treated with or without KM8927.

Please note: Wiley-Blackwell are not responsible for the content or functionality of any supporting materials supplied by the authors. Any queries (other than missing material) should be directed to the corresponding author for the article.

Brain Tumor Pathol (2011) 28:59–64
DOI 10.1007/s10014-010-0009-x

CASE REPORT

Epithelioid glioblastoma changed to typical glioblastoma: the methylation status of MGMT promoter and 5-ALA fluorescence

Shingo Tanaka · Mitsutoshi Nakada · Yutaka Hayashi · Satoko Nakada · Seiko Sawada-Kitamura · Natsuki Furuyama · Tomohide Suzuki · Tomoya Kamide · Yasuhiko Hayashi · Seiji Yano · Jun-ichiro Hamada

Received: 20 July 2010 / Accepted: 12 October 2010 / Published online: 25 December 2010

Abstract A 55-year-old man was admitted to our hospital complaining of left hemiparesis. Magnetic resonance imaging (MRI) showed a smooth ring-like enhanced cystic tumor in the right parietal lobe. He underwent gross total resection of the tumor under neuronavigation and 5-aminolevulinic acid (5-ALA) fluorescence guiding method. Histopathological examination of the tumor showed small cells formed epithelioid solid nests with some focus of duct-like structure. On the basis of the MRI and operative and histological findings, this tumor was diagnosed as a metastatic poorly differentiated carcinoma, although the primary cancer could not be detected by metastatic work-ups. Afterward, this tumor recurred repeatedly. Histopathological examination of specimen from the fourth surgery indicated that the tumor was a glioblastoma (GBM). In the review of the histology and immunohistochemistry of the first tumor, atypical fibrillary cells were seen between solid nests and positive for glial fibrillary acidic protein, therefore the tumor was retrospectively diagnosed as epithelioid GBM. We assessed whether the changes in histopathology were accompanied by changes in the methylation status of O6-methylguanine methyltransferase (MGMT) promoter and the status of 5-ALA fluorescence. The methylation status of the MGMT promoter was found to have changed from methylated to unmethylated and 5-ALA fluorescence became positive along with the histological change.

Keywords Epithelioid GBM · MGMT · Methylation · 5-ALA

Abbreviations

CT	Computed tomography
MRI	Magnetic resonance imaging
GBM	Glioblastoma
5-ALA	5-Aminolevulinic acid
PPIX	Protoporphyrin IX
MGMT	O6-Methylguanine methyltransferase

Introduction

Glioblastoma (GBM) is the most malignant astrocytic tumor of the central nervous system. The diagnosis of this tumor can be difficult when tumor cells resemble a metastatic brain tumor. An example of GBM showing adenoid structures was first reported by Kepes et al., and 75 additional cases of GBM showing epithelioid structures or epithelial metaplasia have since been reported [1–8]. Our patient was initially suspected to have a metastatic carcinoma owing to the magnetic resonance imaging (MRI), operative, and histopathological findings. However, as the

S. Tanaka · M. Nakada (✉) · Y. Hayashi · N. Furuyama · T. Suzuki · T. Kamide · Y. Hayashi · J. Hamada
Division of Neuroscience, Department of Neurosurgery, Graduate School of Medical Science, Kanazawa University, 13-1 Takara-machi, Kanazawa, Ishikawa 920-8641, Japan
e-mail: nakada@ns.m.kanazawa-u.ac.jp

S. Nakada
Department of Pathology and Laboratory Medicine, Kanazawa Medical University, 1-1 Daigaku, Uchinada, Kahoku, Ishikawa 920-0293, Japan

S. Sawada-Kitamura
Pathology Section, Kanazawa University Hospital, 13-1 Takara-machi, Kanazawa, Ishikawa 920-8641, Japan

S. Yano
Division of Medical Oncology, Cancer Research Institute, Kanazawa University, Kanazawa, Japan

clinical course progressed, the histological features of the tumor changed to those of typical GBM. In reviewing the histology of the first tumor, glial fibrillary acidic protein (GFAP)–positive astrocytic cells were seen between epithelioid structures. Our patient was therefore diagnosed as epithelioid GBM. In this report, we discuss the relationships among the histological change, the methylation status of O6-methylguanine methyltransferase (MGMT) promoter, and the status of 5-aminolevulinic acid (5-ALA)-induced protoporphyrin IX (PPIX) fluorescence.

Clinical summary and pathological findings

A 55-year-old man presented with left hemiparesis in January 2008. He visited our hospital and underwent MRI, which revealed a right parietal lobe cystic mass lesion of about 5 cm in diameter (Fig. 1). The differential diagnosis, based on the MRI identification of a smooth ring-like enhancement, was a metastatic brain tumor rather than GBM, although metastatic work-up, which included enhanced computed tomography (CT) of the whole body and tests for serum tumor markers, yielded negative results. The tumor was removed, resulting in improvement of the left hemiplegia. Operative tools for tumor removal included the neuronavigation system and the 5-ALA fluorescence guiding method. The operative findings were relatively clear tumor borders and absence of 5-ALA fluorescence. The histopathological findings were solid nests cohesively formed by small round cells with atypical nuclei, epithelioid structures with some foci of duct-like structure, and necrosis (Fig. 2a, b). The diagnosis was metastatic poorly differentiated carcinoma. Other tests for metastatic work-up, such as positron-emission tomography (PET), ^{67}Ga-citrate scintigraphy, MRI, and CT of the whole body, resulted in negative findings.

Follow-up MRI conducted 5 and 13 months after the first surgery showed recurrence of the tumor (Fig. 1). At both times, tumor recurred after the removal was macroscopically totally removed using the same method as the first surgery. The histology of the second and third tumors showed small round cells densely proliferated as solid nest in addition to the epithelial structure seen in the first tumor (Fig. 2c). In immunohistochemical study on the 2nd tumor, tumor cells forming solid nests were positive for epithelial markers, cytokeratins such as AE1/AE3 and CK7 (Fig. 2d), negative for CK20, negative for TTF-1 which is a thyroid and lung cancers' marker, focally positive for CEA, and positive for neuroendocrine markers such as CD56 (Fig. 2e) and synaptophysin. Based on these findings, second and third tumors were diagnosed as metastatic poorly differentiated adenocarcinoma with neuroendocrine differentiation. Subsequently, radiation therapy was performed (after the second surgery: whole brain 30 Gy + local 20 Gy; after the third surgery: local 30 Gy) (Fig. 1). The irradiated area after the third surgery did not overlap with the area irradiated after the second surgery.

After 15 and 23 months from the first resection, MRI revealed recurrences close to the resected tumor cavity (Fig. 1). The recurrent tumors exhibited 5-ALA fluorescence (Fig. 3). The histopathological characteristics of the recurrent tumor obtained after the fourth surgery were identical to those of GBM, which was hypercellular proliferation of the atypical spindle, fibrillary or polygonal cells, mitosis, and microvascular proliferation. Radiation effects were also observed partially, such as radiation necrosis and hyalinization of small vessels, but no evidence of epithelial structures like carcinoma were seen in the first to third tumors (Fig. 2f, g). Immunohistochemical study showed that tumor cells were negative for AE1/AE3 and positive for GFAP. The methylation status of the MGMT promoter was determined using a methylation-specific polymerase chain reaction (PCR) method [9, 10]. The MGMT promoter of this typical GBM was unmethylated (Fig. 3). The patient was conventionally treated with

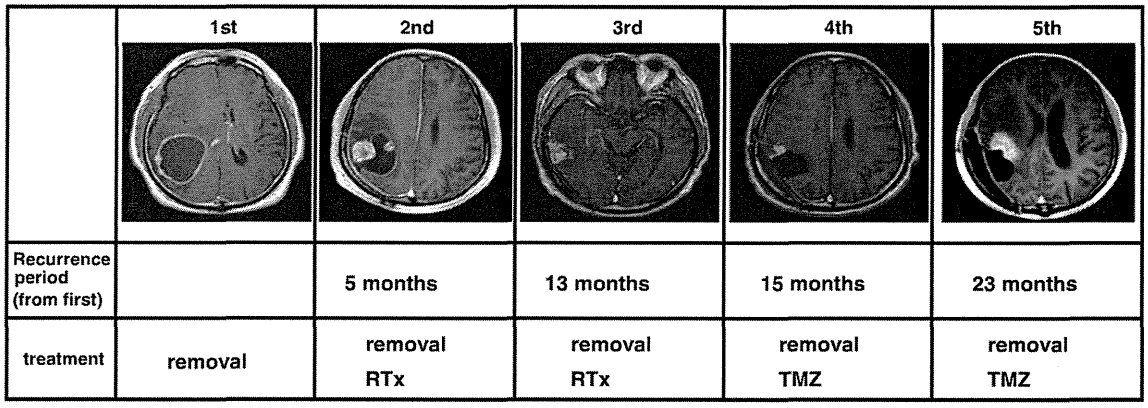

Fig. 1 The clinical course of the case is shown. Gadolinium-enhanced T1-weighted magnetic resonance images of the tumor (*upper column*), time to recurrence from the first surgery (*middle column*), and treatment administered (*lower column*) are indicated. (RTx: radiotherapy)

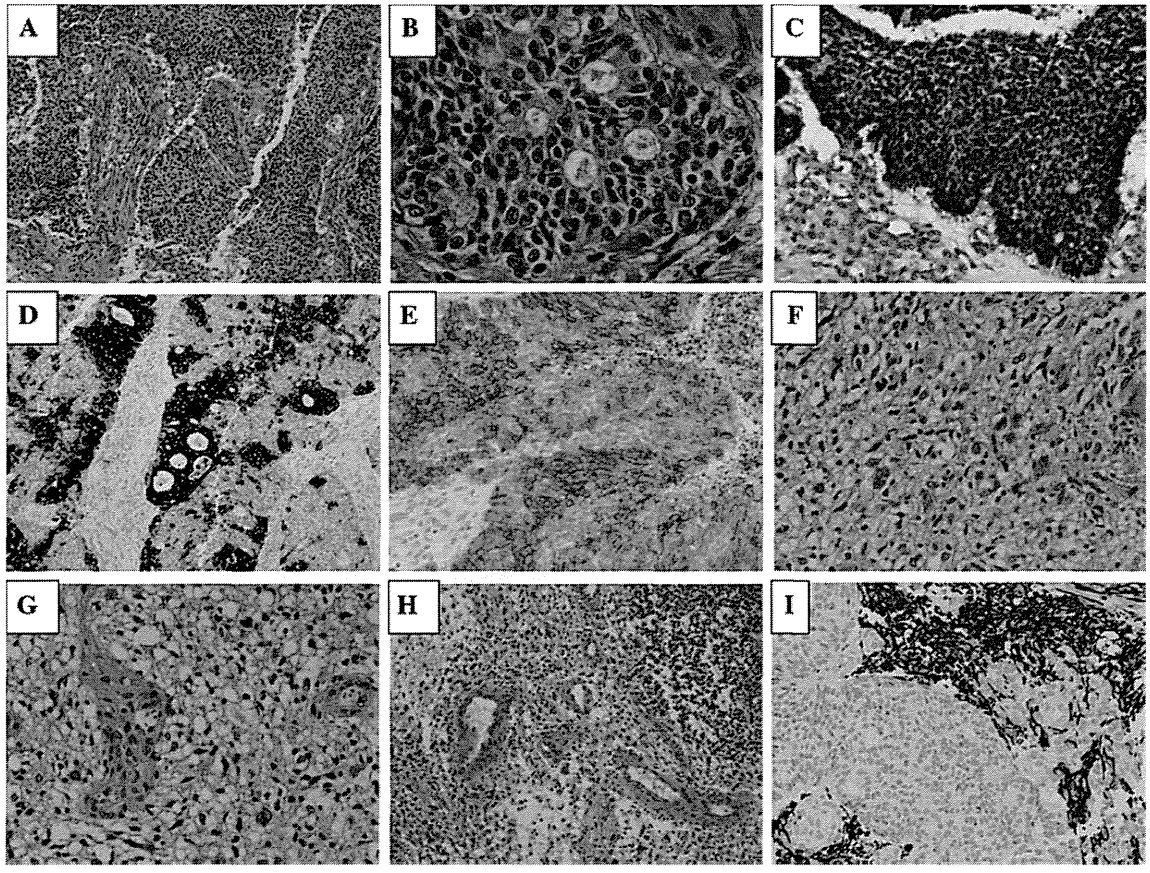

Fig. 2 Histological examination of the surgical specimen obtained from the first (**a**, **b**, **h**, **i**), 2nd (**c**–**e**), and 4th operation (**f**, **g**). **a** Hematoxylin–eosin staining of the 1st tumor; small round cells cohesively form solid nests, epithelioid foci, which resembles carcinoma, but proliferation of spindle cells can also be seen between the solid nests (×100). **b** Some foci of the ductular structure are seen in solid nests of small cells. Tumor cells have round to polygonal, well-defined cytoplasm, round and hyperchromatic nuclei, and prominent nucleoli (×400). **c** Hematoxylin–eosin staining of the 2nd tumor; small round cells densely proliferate as a solid nest, which reminds of neuroendocrine feature. **d** Immunohistochemistry of cytokeratin 7 (CK7) on the 2nd tumor; epithelioid parts including ductular areas of tumor are positive (×400). **e** Immunohistochemistry of CD56 on the 2nd tumor; a dense solid nest of small round cells are focally positive, which suggests neuroendocrine feature (×400). **f** Hematoxylin–eosin staining of the 4th tumor; atypical fibrillary to polygonal astrocytic cells were seen densely. Note that some cells have pleomorphic nuclei. **g** Hematoxylin–eosin staining of the 4th tumor; microvascular proliferation is also seen (×400). **h** Hematoxylin–eosin staining of the 1st tumor; besides solid epithelial parts, proliferation of spindle cells and microvascular proliferation are seen. **i** Immunohistochemistry of GFAP on the 1st tumor; epithelioid parts of the tumor are negative, but most spindle cells are positive for GFAP (×100)

	1st	2nd	3rd	4th	5th
Histology	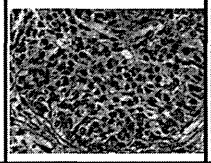	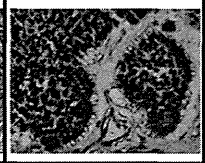	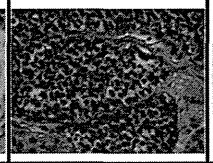	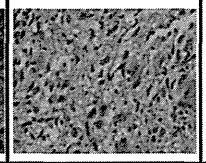	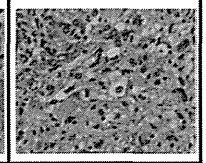
MGMT promoter	methylated	methylated	methylated	unmethylated	unmethylated
5-ALA fluorescence	–	–	–	+	+

Fig. 3 Summary of tumor histology (*upper column*), status of MGMT promoter (*middle column*), and 5-ALA fluorescence (*lower column*)

adjuvant chemotherapy with temozolomide (TMZ) after the fourth surgery.

We retrospectively reviewed the histology and performed additional immunohistochemistry on the first tumor because the first, second, and third tumors were suspected to be histoarchitectural variations of GBM. The first tumor was a mixed pattern of epithelioid structures that was negative for GFAP and the fibrillary cells surrounding epithelioid structures, which were positive for GFAP (Fig. 2h, i). In addition, the original site of the tumor was not identified by metastatic work-ups. Therefore, the final diagnosis of this tumor was epithelioid GBM rather than metastatic brain tumor. The MGMT promoter was methylated in tissues drawn from the first, second, and third surgeries.

Methods

Immunohistochemistry

Immunohistochemical analyses were performed on the 4% paraformaldehyde-fixed, paraffin-embedded tissue. Primary antibodies used were as follows: cytokeratin AE1/3 (AE1/3) (DAKO Japan Co., Kyoto, Japan; 1:100 dilution), cytokeratin 7 (CK7) (DAKO Japan Co.; 1:75 dilution), GFAP (DAKO Japan Co.; 1:500 dilution), nestin (BD biosciences, San Jose, CA, USA; 1:500 dilution). Immunohistochemical staining was performed using the avidin–biotin immunoperoxidase method as previously described [11]. Appropriate positive and negative controls were performed with each immunostaining.

Methylation-specific polymerase chain reaction (MSP) assay

The status of MGMT promoter methylation can be evaluated by MSP assay as previously described [9, 10]. In our modified method, sodium bisulfite modification and purification of 200 ng of the purified DNA was performed using MSP kit^{TM} (QIAGEN Inc.). The modification of DNA was performed by PCR. Universal methylated DNA (CpG genome^{TM} Chemicon International, Temecula, CA, USA) and U138MG cell lines were used as the methylated and unmethylated controls, respectively. PCR was carried out in a nested, two-stage PCR approach. The PCR products were separated on a 3% agarose gel. Amplified PCR products were electrophoresed in 3% agarose gels and visualized with ethidium bromide.

Quantitative real-time PCR (QRT-PCR)

QRT-PCR was performed in a LightCycler (Roche Diagnostics, Indianapolis, IN) as described previously [11]. PCR was done with the following primers: CD133 (NM_006017.1): sense 5′-TTGTGGCAAATCACCAGG TA-3′, antisense 5′-TCAGATCTGTGAACGCCTTG-3′ (amplicon size 162 bp); and β-actin (NM_001101): sense 5′-CTACAATGAGCTGCGTGTGGC-3′, antisense 5′-CA GGTCCAGACGCAGGATGGC-3′ (amplicon size, 271 bp). The LightCycler analysis software was used to analyze the PCR data as described previously [11].

Discussion

Epithelioid GBM, which is also known as adenoid GBM or GBM with epithelial metaplasia, was first reported by Kepes et al. [1]. Seventy-five cases of epithelioid GBM have been reported to date [1–8]. Epithelioid GBM has epithelioid features like ductular, glandular, or squamoid patterns besides astrocytic parts. These epithelioid foci have astrocytic nature immunohistochemically positive for GFAP, even which reduced the positivity, and also epithelial nature which shows immunoreactivity for cytokeratins such as AE1/3, CK7, and CK20 [1–8, 12]. Because its histopathological features mimic those of metastatic brain adenocarcinoma, this GBM is frequently misdiagnosed; the true diagnosis is occasionally revealed on autopsy [1, 4, 5]. Brain metastases of an unknown primary tumor should arouse suspicion of an epithelioid GBM [3, 8]. Our patient was initially diagnosed as metastatic poorly differentiated carcinoma, but repeated recurrences caused us to review the histology and immunohistochemistry of the first tumor, which revises the diagnosis to epithelioid GBM. GFAP staining of the first tumor on the first analysis must have led us to make the true diagnosis earlier, even when the primary site of metastatic carcinoma had not been detected by work-ups.

We eventually diagnosed this tumor as epithelioid GBM because of the three reasons described below. First, the histology and immunohistochemical findings of the first, second, and third tumors resembled those of epithelioid GBM. Second, all the tests in the metastatic work-up yielded negative results throughout the clinical course. Third, our patient might have had a radiation-induced GBM because the tumor arose in the field of irradiation. However, the rapid tumor recurrence within 10 months does not satisfy Cahan's criteria for radiation-induced tumors [13]. Two distinct tumors are another possibility. To the best of our knowledge, both GBM and metastatic brain tumor have never been reported in a single patient.

We should consider the mechanism underlying the change in the histopathological features of the tumor from the fourth surgery from epithelioid GBM to common GBM. Current research indicates that GBM originates from glioma-initiating cells, which have self-renewal and

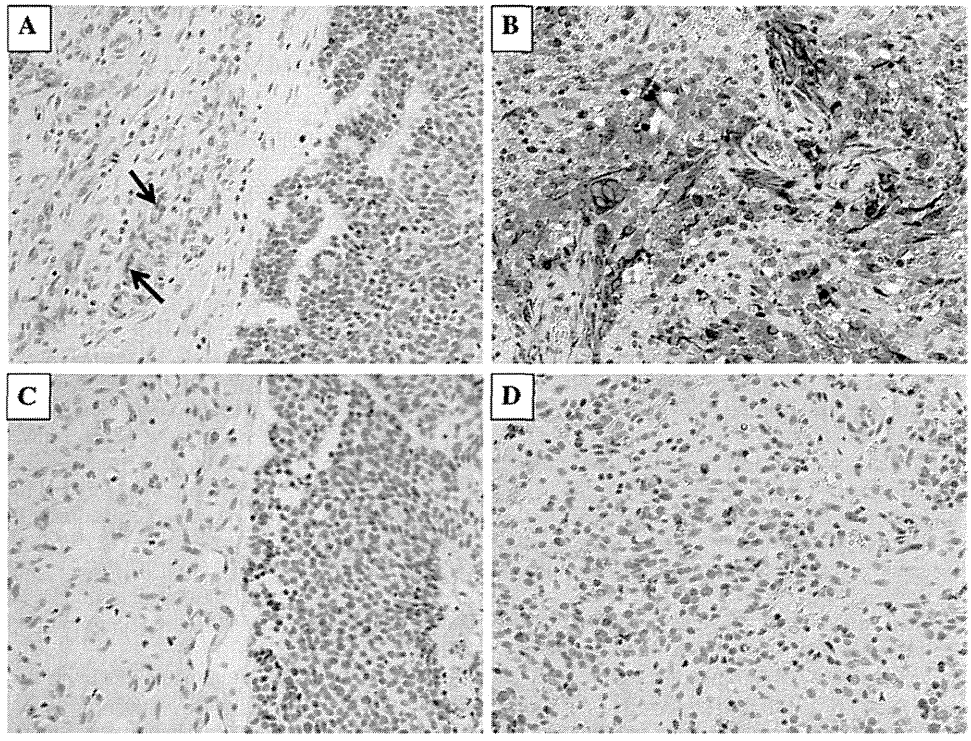

Fig. 4 Immunohistochemistry of nestin in surgical specimen of second (**a**, **c**) and fourth operation (**b**, **d**). **a** Spindle cells (*arrow*) surrounding epithelioid parts were weakly positive (×200). **b** Tumor cells were diffusely positive (×200). **c**, **d** No immunoreactivity was seen in a section treated with a non-specific isotype control instead of the nestin antibody (×200)

multi-lineage potential and are resistant to chemo- and radiotherapy [14, 15]. Nestin and CD133 have been suggested to be tumor-initiating cell markers in malignant glioma [16–18]. The expression of nestin in this case was assessed by immunohistochemistry. Nestin showed moderate staining in tumor cells surrounding epithelioid parts obtained from the 2nd surgery (Fig. 4a). Nestin was found to be remarkably expressed in numerous tumor cells obtained from the 4th surgery (Fig. 4b). The expression level of CD133 was higher in the 5th tumor tissue than in the 1st tumor tissues by QRT-PCR (33-fold). From these data, it is reasonable to speculate that the population of glioma-initiating cells might have persisted after radiotherapy in our patient, and this population might have differentiated to a glial component rather than an epithelial component.

The standard therapy for GBM is surgery followed by TMZ administration with concurrent radiotherapy [19]. The methylation of the MGMT promoter has been reported as a predictive marker of sensitivity to alkylating agents such as TMZ and a prognostic factor in GBM patients [20]. The methylation status of the MGMT promoter in epithelioid GBM has never been reported. The MGMT promoter was unmethylated in the 4th and 5th tumors, which showed histologically common GBM. It is possible that radiotherapy affected this change; a study has reported radiation-induced unmethylation of the MGMT promoter in GBM patients [21]. It has also been reported that glioma-initiating cells express high levels of MGMT [14]. In our patient, nestin and CD133 expression level in the 4th and 5th tumors were higher than that in the 1st and 2nd tumors. Taken together, these results lead us to propose that the unmethylation of the MGMT promoter observed in the fourth and fifth tumors might be a result of both the radiotherapy itself and the glioma-initiating cells that persisted after radiotherapy.

5-ALA fluorescence-guided neurosurgery has been reported as a method that enables intraoperative identification of tumor borders and more effective resection of tumors [22, 23]. This technique is now widely used for GBM removal. GBM is particularly known to be positive for 5-ALA fluorescence [23]. In contrast, metastatic brain tumors are negative for 5-ALA fluorescence [24]. This study represents the first example where epithelioid GBM was remarkably negative in 5-ALA fluorescence but common GBM histological-changed was positive. In our case, histology reflected 5-ALA fluorescence of tumors.

We have observed a rare case of epithelioid GBM. The histological characteristics of this tumor changed from epithelioid GBM to common GBM during the clinical course. This change might be associated with altered methylation status of the MGMT promoter and the appearance of 5-ALA fluorescence.

References

1. Kepes JJ, Fulling KH, Garcia JH (1982) The clinical significance of "adenoid" formations of neoplastic astrocytes, imitating

metastatic carcinoma, in gliosarcomas. A review of five cases. Clin Neuropathol 1:139–150
2. Akimoto J, Namatame H, Haraoka J et al (2005) Epithelioid glioblastoma: a case report. Brain Tumor Pathol 22:21–27
3. Miyata S, Sugimoto T, Kodama T et al (2005) Adenoid glioblastoma arising in a patient with neurofibromatosis type-1. Pathol Int 55:348–352
4. Mork SJ, Rubinstein LJ, Kepes JJ (1988) Patterns of epithelial metaplasia in malignant gliomas. I. Papillary formations mimicking medulloepithelioma. J Neuropathol Exp Neurol 47:93–100
5. Mork SJ, Rubinstein LJ, Kepes JJ et al (1988) Patterns of epithelial metaplasia in malignantgliomas. II. Squamous differentiation of epithelial-like formations in gliosarcomas and glioblastomas. J Neuropathol Exp Neurol 47:101–118
6. Shintaku M, Hirano A, Llena JF (1988) Fine structure of glioblastoma multiforme with "adenoid formation". No Shinkei Geka 16:997–1003
7. Shintaku M, Nakatsu S, Okamoto S (2000) "Adenoid" glioblastoma. No Shinkei Geka 28:359–365
8. Rodriguez FJ, Scheithauer BW, Giannini C et al (2008) Epithelial and pseudoepithelial differentiation in glioblastoma and gliosarcoma: a comparative morphologic and molecular genetic study. Cancer 113:2779–2789
9. Kamide T, Nakada M, Hayashi Y et al (2010) Radiation-induced cerebellar high-grade glioma accompanied by meningioma and cavernoma 29 years after the treatment of medulloblastoma: a case report. J Neurooncol 2010 Mar 31 [Epub ahead of print]
10. Palmisano WA, Divine KK, Saccomanno G et al (2000) Predicting lung cancer by detecting aberrant promoter methylation in sputum. Cancer Res 60:5954–5958
11. Yoshida Y, Nakada M, Sugimoto N et al (2010) Sphingosine-1-phosphate receptor type 1 regulates glioma cell proliferation and correlates with patient survival. Int J Cancer 126:2341–2352
12. Ozolek JA, Finkelstein SD, Couce ME (2004) Gliosarcoma with epithelial differentiation: immunohistochemical and molecular characterization. A case report and review of the literature. Mod Pathol 17:739–745
13. Balasubramaniam A, Shannon P, Hodaie M et al (2007) Glioblastoma multiforme after stereotactic radiotherapy for acoustic neuroma: case report and review of the literature. Neuro Oncol 9:447–453
14. Pistollato F, Abbadi S, Rampazzo E et al (2010) Intratumoral hypoxic gradient drives stem cells distribution and MGMT expression in glioblastoma. Stem Cells 28(5):851–862
15. Singh SK, Hawkins C, Clarke ID et al (2004) Identification of human brain tumour initiating cells. Nature 432:396–401
16. Zhang M, Song T, Yang L et al (2008) Nestin and CD133: valuable stem cell-specific markers for determining clinical outcome of glioma patients. J Exp Clin Cancer Res 27:85
17. Strojnik T, Rosland GV, Sakariassen PO et al (2007) Neural stem cell markers, nestin and musashi proteins, in the progression of human glioma: correlation of nestin with prognosis of patient survival. Surg Neurol 68:133–143
18. Tamura K, Aoyagi M, Wakimoto H et al (2010) Accumulation of CD133-positive glioma cells after high-dose irradiation by gamma knife surgery plus external beam radiation. J Neurosurg 113:310–318
19. Stupp R, Mason WP, van den Bent MJ et al (2005) Radiotherapy plus concomitant and adjuvant temozolomide for glioblastoma. N Engl J Med 352:987–996
20. Brandes AA, Franceschi E, Tosoni A et al (2010) O(6)-Methylguanine DNA-methyltransferase methylation status can change between first surgery for newly diagnosed glioblastoma and second surgery for recurrence: clinical implications. Neuro Oncol 12:283–288
21. Parkinson JF, Wheeler HR, Clarkson A et al (2008) Variation of O(6)-methylguanine-DNA methyltransferase (MGMT) promoter methylation in serial samples in glioblastoma. J Neurooncol 87:71–78
22. Stummer W, Pichlmeier U, Meinel T et al (2006) Fluorescence-guided surgery with 5-aminolevulinic acid for resection of malignant glioma: a randomised controlled multicentre phase III trial. Lancet Oncol 7:392–401
23. Stummer W, Novotny A, Stepp H et al (2000) Fluorescence-guided resection of glioblastoma multiforme by using 5-aminolevulinic acid-induced porphyrins: a prospective study in 52 consecutive patients. J Neurosurg 93:1003–1013
24. Utsuki S, Miyoshi N, Oka H et al (2007) Fluorescence-guided resection of metastatic brain tumors using a 5-aminolevulinic acid-induced protoporphyrin IX: pathological study. Brain Tumor Pathol 24:53–55

Research article

Lipoxygenase mediates invasion of intrametastatic lymphatic vessels and propagates lymph node metastasis of human mammary carcinoma xenografts in mouse

Dontscho Kerjaschki,[1,2] Zsuzsanna Bago-Horvath,[1,2,3] Margaretha Rudas,[1,2,3] Veronika Sexl,[4] Christine Schneckenleithner,[4] Susanne Wolbank,[5] Gregor Bartel,[1] Sigurd Krieger,[1] Romana Kalt,[1] Brigitte Hantusch,[1,2] Thomas Keller,[1] Katalin Nagy-Bojarszky,[1] Nicole Huttary,[1] Ingrid Raab,[1] Karin Lackner,[1] Katharina Krautgasser,[1] Helga Schachner,[1] Klaus Kaserer,[1] Sandra Rezar,[1] Sybille Madlener,[1] Caroline Vonach,[1] Agnes Davidovits,[1] Hitonari Nosaka,[1] Monika Hämmerle,[1] Katharina Viola,[1] Helmut Dolznig,[1] Martin Schreiber,[6] Alexander Nader,[7] Wolfgang Mikulits,[2,8] Michael Gnant,[2,3,9] Satoshi Hirakawa,[10] Michael Detmar,[11] Kari Alitalo,[12] Sebastian Nijman,[13] Felix Offner,[14] Thorsten J. Maier,[15] Dieter Steinhilber,[15] and Georg Krupitza[1,2]

[1]Clinical Institute of Pathology, [2]Comprehensive Cancer Center, [3]Austrian Breast and Colorectal Cancer Study Group (ABCSG), and [4]Institute of Pharmacology, Medical University of Vienna, Vienna, Austria. [5]Ludwig Boltzmann Institute for Experimental and Clinical Traumatology, Vienna, Austria. [6]Department of Gynaecology, Medical University of Vienna, Vienna, Austria. [7]Pathology Institute, Hanusch Hospital, Vienna, Austria. [8]Institute of Cancer Research and [9]Department of Surgery, Medical University of Vienna, Vienna, Austria. [10]Department of Dermatology, Ehime University Graduate School of Medicine, Ehime, Japan. [11]Department of Pharmacogenomics, Swiss Federal Institute of Technology ETH-Zurich, Zurich, Switzerland. [12]Molecular/Cancer Biology Laboratory, Biomedicum Helsinki, University of Helsinki, Helsinki, Finland. [13]Ce-M-M-Research Center for Molecular Medicine of the Austrian Academy of Sciences, Vienna, Austria. [14]Institute for Pathology, LKH Feldkirch, Austria. [15]Institute of Pharmaceutical Chemistry/ZAFES, Frankfurt/Main, Germany.

In individuals with mammary carcinoma, the most relevant prognostic predictor of distant organ metastasis and clinical outcome is the status of axillary lymph node metastasis. Metastases form initially in axillary sentinel lymph nodes and progress via connecting lymphatic vessels into postsentinel lymph nodes. However, the mechanisms of consecutive lymph node colonization are unknown. Through the analysis of human mammary carcinomas and their matching axillary lymph nodes, we show here that intrametastatic lymphatic vessels and bulk tumor cell invasion into these vessels highly correlate with formation of postsentinel metastasis. In an *in vitro* model of tumor bulk invasion, human mammary carcinoma cells caused circular defects in lymphatic endothelial monolayers. These circular defects were highly reminiscent of defects of the lymphovascular walls at sites of tumor invasion in vivo and were primarily generated by the tumor-derived arachidonic acid metabolite 12S-HETE following 15-lipoxygenase-1 (ALOX15) catalysis. Accordingly, pharmacological inhibition and shRNA knockdown of ALOX15 each repressed formation of circular defects in vitro. Importantly, ALOX15 knockdown antagonized formation of lymph node metastasis in xenografted tumors. Furthermore, expression of lipoxygenase in human sentinel lymph node metastases correlated inversely with metastasis-free survival. These results provide evidence that lipoxygenase serves as a mediator of tumor cell invasion into lymphatic vessels and formation of lymph node metastasis in ductal mammary carcinomas.

Introduction

A tumor's metastatic potential is determined by complex and specific genetic gains and/or losses of function that enable tumor cells to emigrate from their primary site to access the blood or lymphatic vasculature and to form premetastatic niches in target organs that provide the essential "soil" for "seeding" of incoming tumor cells (1). Despite the obvious clinical relevance of these events, relatively little is currently known about the underlying mechanisms. For example, only some aspects of niche formation in distant organs have been identified; these include local accumulation of bone marrow–derived cells, fibronectin deposition (2), and interactions between tumor cells and thrombocytes (3).

Whether tumors metastasize initially into lymph nodes or are distributed by hematogenous dissemination into distant organs remains a matter for debate, and there is experimental evidence for each hypothesis (4–6). One view holds that metastatic tumor cells colonize distant organs via the blood stream either from lymph nodes ("metastasis from metastasis") (7) or by cross seeding from the primary tumor by recirculation (8). Alternatively, clonogenic tumor cells, presumably with stem cell–like characteristics, could disseminate simultaneously at an early time point from primary tumors into both the blood and lymphatic vasculature and then develop metastases asynchronously in both compartments (9). Although currently evidence is accumulating in favor of the latter hypothesis (5), it falls short of explaining why the number of regional lymph nodes affected by metastases most accurately predicts the general extent of metastatic spreading and overall clinical outcome, for

Conflict of interest: The authors have declared that no conflict of interest exists.
Citation for this article: *J Clin Invest.* 2011;121(5):2000–2012. doi:10.1172/JCI44751.

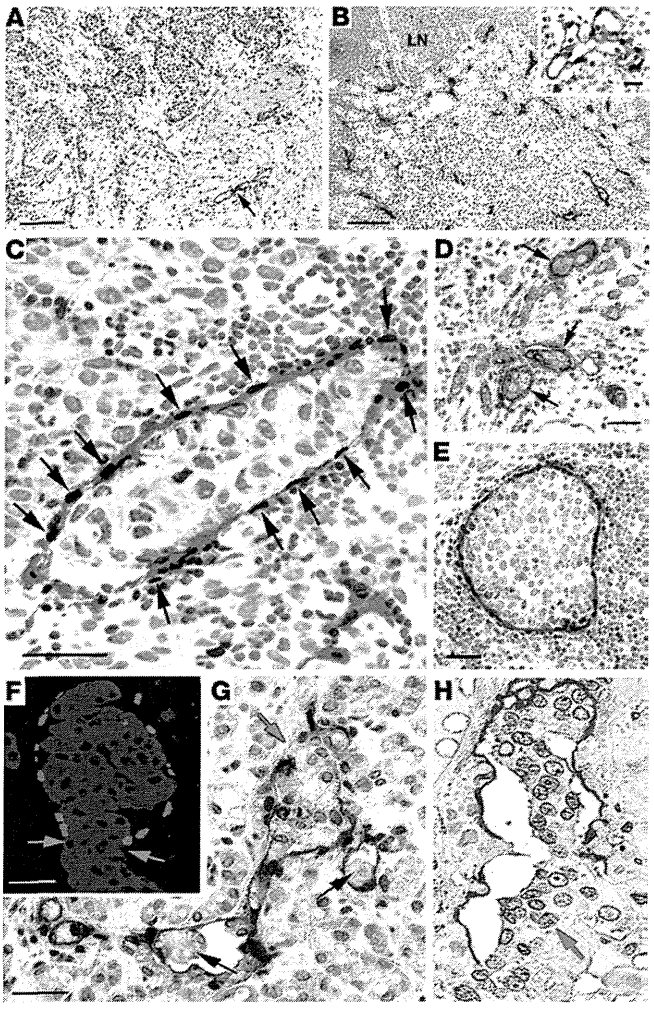

Figure 1
Intrametastatic lymphangiogenesis and tumor cell invasion into lymphatic vessels in sentinel lymph nodes of human ductal mammary carcinomas with postsentinel metastasis. Lymphatic endothelial cells are localized by double labeling for podoplanin (red) and PROX1 (black) in **A–C** and **E**. (**A**) In a primary ductal carcinoma, lymphatic vessels are localized in the peritumoral stroma (arrow). The tumor border is marked by a green line. (**B**) Sentinel lymph node metastasis of the same carcinoma as in part **A**, with dense intrametastatic lymphatic vascularization. LN, residual lymph node parenchyma. Insert, FLT4 (red) in an intrametastatic lymphatic vessel (PROX1, black). (**C**) High-power view of an intrametastatic lymphatic vessel with podoplanin$^+$ lymphatic endothelial cells and PROX1-expressing nuclei (arrows). The vessel contains a tumor embolus and is surrounded by mononuclear inflammatory or tumor cells. (**D**) Keratin$^+$ tumor cell emboli (brown) within intrametastatic lymphatic vessels with podoplanin$^+$ endothelial cells (red). (**E**) Large tumor embolus completely filling the lumen of an intrametastatic lymphatic vessel. (**F**) Aggregate of keratin$^+$ carcinoma cells disrupts an intrametastatic lymphatic vessel that is outlined by a single line of PROX1$^+$ nuclei (red). The margins of the vessel's rupture are indicated by green arrows. (**G** and **H**) Embolic tumor cell clusters (black arrows) within a branched intrametastatic lymphatic vessel, and a focal disruption of the lymphatic vascular wall by a bulk of aggregated tumor cells (green arrow). The lymphatic vessel's walls are composed of a single endothelial layer. Scale bars: 100 μm; 25 μm (insert).

example, in mammary carcinomas. This well-established fact is reflected in clinically validated and diagnostically indispensable consensus systems used in routine histopathological mammary tumor staging (10, 11). Testing these hypotheses, which are not mutually exclusive, depends on better understanding of the so-far elusive molecular mechanisms that determine the initial tumor cells' specific preference for invasion of blood or lymphatic vessels to reach their respective target organs.

Here we have systematically analyzed the lymphometastatic properties of human mammary carcinomas. These have distinct advantages for such studies, including the anatomically conserved lymphatic draining patterns of the human breast (12) and their repetitive pattern of metastatic spreading. Thus, most mammary carcinomas form their initial metastasis in up to 3 axillary lymph node or nodes that receive afferent lymph from the tumor and peritumoral tissue and are designated as "sentinel lymph nodes." Further metastatic progression occurs by successive colonization of the postsentinel lymph nodes in the axillary basin. Previous work has shown that lymphangiogenesis in sentinel lymph node metastases correlates with postsentinel tumor spreading (13). In this study, we have addressed the mechanisms underlying this process, using immunohistochemistry with selective lymphatic endothelial markers (podoplanin, LYVE1, and PROX1) (14–16), in vitro models, and xenograft tumors. The findings are compatible with a context-specific reaction of lymphatic endothelial cells with tumor-derived products of lipoxygenases that is critical for tumor cell entry into the lymphatic vessel and metastatic spreading from the sentinel to postsentinel lymph nodes. The results also shed light on the fact that different tumor types use different means to invade intrametastatic lymphatics.

Results

Intrametastatic lymphatic carcinosis. We localized lymphatic endothelial cells in 104 precisely matched primary ductal and lobular mammary carcinomas (stages pT1c, N0, or N1a, or pooled stages N2 and N3; ref. 11 and Supplemental Table 1; supplemental material available online with this article; doi:10.1172/JCI44751DS1) and in their corresponding sentinel and postsentinel axillary lymph nodes (Figure 1). Lymphatic vessels were restricted to the peritumoral stroma (17) in all the primary carcinomas. In contrast, the sentinel lymph node metastases of these tumors were often endowed with lymphatic vessels connected to those in the residual sentinel lymph node's parenchyma (Supplemental Figure 1). Their endothelial cells expressed the major lymphatic markers FLT4 (VEGFR3), podoplanin, PROX1, and, with some variability, also LYVE1, as reported (18). The density of intrametastatic lymphatics and their endothelial mitotic rate were more than 2-fold higher than those in residual lymph nodes (Supplemental Figure 2). The metastatic tumor cells were a major source of the lymphangiogenic factors

Table 1
Characterization of tumors and patients' outcome

pN Stage	Primary tumor stage pT1c diameter	Peritumoral carcinosis primary tumor	Grading	Grading (%)	Intrametastatic carcinosis	Local recurrence	Distant organ metastasis	Death	Follow-up period (months)
Ductal carcinoma									
pN1a a (n = 39)	1.8 ± 0.4 cm	19 (49%)	G1	2 (5%)	0 of 39 (0%)	0	5 (13%)	3 (8%)	54
			G2	22 (56%)					
			G3	15 (39%)					
pN2/3 (n = 20)	1.9 ± 0.3 cm	16 (65%)	G1	3 (15%)	20 of 20 (100%)	2 (10%)	5 (25%)	5 (25%)	56
			G2	8 (40%)					
			G3	9 (45%)					
Lobular carcinoma									
pN1a (n = 17)	1.9 ± 0.35 cm	4 (24%)	G1	0	0 (0%)	0	0	0	55
			G2	14 (82%)					
			G3	3 (18%)					
pN2/3 (n = 12)	1.8 ± 0.6 cm	5 (42%)	G1	0	6 of 12 (50%)	1 (8%)	3 (25%)	3 (25%)	57
			G2	10 (83%)					
			G3	2 (17%)					

Mean age, 58.9 ± 12.8 years. pT1c, primary tumors with diameters between 1–2 cm; pN1a, metastasis in 1–3 axillary lymph node(s), at least 4 larger than 2 mm in greatest diameter; pN2/3, metastases in more than 4 (ipsilateral) lymph nodes, at least 1 larger than 2 mm in greatest diameter. Data applies to all 3 tumor grades.

VEGFC and VEGFA (19), and their expression in the metastasis frequently exceeded that of the corresponding primary tumors (Supplemental Figure 3) and that of mononuclear cells (20) in the adjacent residual lymph node parenchyma or in naive lymph nodes (data not shown). These results suggest that metastatic tumor colonies provide lymphangiogenic factors and coopt the sentinel lymph node's premetastatic lymphatics and extend them by intrametastatic lymphangiogenesis.

We identified carcinoma cell emboli of various sizes within the intrametastatic lymphatic vessels of sentinel lymph nodes (Figure 1). Emboli were present in 100% (20 of 20) of ductal carcinomas with postsentinel lymph node involvement (Table 1), similar to our recent findings in extramammary Paget carcinomas (21). Strikingly, intrametastatic carcinosis was also present in all postsentinel lymph node metastases from individuals with advanced disease (data not shown). In contrast, lymphatic carcinosis was not detected in any of the 56 individuals in whom metastatic tumors were restricted to the sentinel lymph node (Table 1). After mean follow-up of 4.5 years, distant organ metastasis and death were more frequent in the patient group with (25%, 5 of 20 patients) than without intrametastatic lymphatic carcinosis (8%, 3 of 39 patients). The primary tumor's peritumoral lymphatic carcinosis was (statistically nonsignificantly) increased with the incidence of intrametastatic tumor emboli (Table 1). No further correlation of intrametastatic lymphatic carcinosis with luminal, basal, or ERBB2-overexpressing carcinoma subtypes (22) was observed. However, in contrast to ductal carcinomas, we found intrametastatic lymphatic carcinosis only in 50% (6 of 12) of lobular carcinomas with postsentinel lymph node involvement (Table 1). This is in line with previous results showing that the global gene expression of ductal and lobular subtypes differs significantly (23).

Using oligonucleotide arrays, we identified several gene products (DUSP1, RGS1, CYR61, CXCR4, and VEGFC) that were overexpressed in tumor cells of the metastasis compared with primary tumors, and the same discriminatory "markers" were also differentially expressed in intrametastatic lymphatic tumor emboli (Supplemental Figure 4). This indicates that tumor emboli originate from the surrounding metastasis rather than from the primary tumor directly via lymphatics in the premetastatic lymph node.

Bulk invasion of tumor cells into intrametastatic lymphatics. Due to the high density of intrametastatic lymphatics, we frequently observed that tumor cells aggregated into clusters and penetrated in bulk through large discontinuities of the intrametastatic lymphatic's walls (Figure 1). Tumor cell aggregates are located within the vascular lumen, and the vascular walls that border the discontinuity consist of a single endothelial cell layer. This is documented by localization of PROX1 that forms a single "rosary"-like cover around the tumor cells (Figure 1). These histological features are not compatible with surrounding and engulfment of the tumor cell clusters by newly formed lymphatic vessels that would result in a double layer of endothelial cells. Our results favor the interpretation of a direct penetration of the tumor cell aggregates through ruptures in the vascular wall that is also in line with the recent ex vivo observation obtained by video microscopy (24).

An in vitro model of lymphatic invasion. We used an in vitro coculture system to analyze the mechanisms of tumor cell–mediated disruption of lymphatic vessels. This employed spheroids (25, 26) of MCF7 mammary carcinoma cells to reproduce the clusters of cells seen in tumor emboli in vivo. MCF7 cell spheroids remained stable

Table 2
Overexpression of genes in MCF-7 spheroids versus monolayers

Description	Gene	Spheroid/monolayer	*P* value
Gain			
CD44 (Indian blood group)	*CD44*	3.45	0.0039
Intercellular adhesion molecule 1 (CD54)	*ICAM1*	2.67	0.0012
Vascular endothelial growth factor (VEGFA)	*VEGFA*	2.73	0.0100
Selectin L (lymphocyte adhesion molecule 1)	*SELL*	2.45	0.0055
Thrombospondin 2	*THBS2*	2.30	0.0125
Arachidonate 15-lipoxygenase	*ALOX15*	1.89[A]	0.0397
Cadherin 1 type 1, E-cadherin (epithelial)	*CDH1*	1.80	0.0139
Integrin alpha 5 (fibronectin receptor)	*ITGA5*	1.76	0.0370
Loss			
Laminin beta 1	*LAMB1*	–3.87	0.0133
Collagen type XII, alpha 1	*COL12A1*	–4.21	0.0016
Platelet/endothelial cell adhesion molecule (CD31)	*PECAM1*	–1.95	0.0041
Thrombospondin 1	*THBS1*	–1.91	0.0008
Vascular endothelial growth factor C (VEGFC)	*VEGFC*	–1.81	0.0295
Vitronectin	*VTN*	–1.45	0.0559

MCF7 cells were grown as spheroids or as monolayers, and lysed to extract and reverse transcribe RNA for low density arrays (Human Extracellular Matrix and Adhesion Molecules PCR Array; SABiosciences). Genes were identified that are differentially induced or repressed by MCF7 cell spheroid formation and could be related to bulk-like invasion through the lymphatic vasculature. [A]Corresponding gene products were studied in more detail.

for more than 6 hours. When aggregated into spheroids, MCF7 cells changed their gene expression patterns when compared with monolayers and increased their expression of CD44, ICAM1, and VEGFA; they also reduced their expression of matrix components (Table 2). Confluent monolayers of freshly isolated or telomerase "immortalized" (27) human dermal lymphatic endothelial cells were used as surrogates for intrametastatic lymphatics. We found no difference between intra- and extratumoral dermal lymphatics for the expression of several proteins (podoplanin, PROX1, FLT4, biglycan, endoglin, VE-cadherin, variably CD34, and LYVE1) (Supplemental Figure 4), justifying their use for the in vitro studies.

MCF7 spheroids were placed on top of lymphatic endothelial monolayers (Figure 2), which resulted in the highly reproducible formation of circular discontinuities that we designated as circular chemorepellent-induced defects (CCID) in monolayers precisely underneath the MCF7 spheroids. They were highly reminiscent of the defects seen in the lymphovascular walls at sites of tumor cell invasion in vivo. Lymphatic endothelial cells were more than 5 times more sensitive to MCF7 spheroid–induced CCID formation than blood vessel endothelia. CCID formation was not seen using spheroids of the nontumorigenic mammary gland epithelial cell line MCF-10A or human lung fibroblasts (HLFs) (Figure 2).

CCIDs form by migration of lymphatic endothelial cells. Time-lapse videos revealed centrifugal migration of lymphatic endothelial cells strictly beneath the MCF7 spheroids (Figure 2 and Supplemental Video). This correlated also with rearrangement and fragmentation of VE-cadherin in lymphatic endothelial cell junctions at the border of MCF7 spheroid–induced CCIDs (Figure 2). The migratory phenotype of the lymphatic endothelia was confirmed by the localization of the cell movement–associated activated protein phosphatase 1 regulatory inhibitor subunit 12 A (PPP1R12A, MYPT1) (ref. 28 and Figure 2). We discounted a role for apoptosis of lymphatic endothelial cells in the formation of CCIDs by TUNEL and Hoechst 33258 staining both in vitro and in vivo in human sentinel metastases (Supplemental Figure 5).

12(S)-HETE induces CCIDs in lymphatic endothelial cell monolayers. Oligonucleotide array analyses revealed the specific induction of several genes in MCF7 cell spheroids when compared with monolayers, including the hypoxia inducible (29) enzyme 15-lipoxygenase-1 (ALOX15) (Table 2), which metabolizes arachidonic acid to 12[S]-hydroxy-eicosatetraenoic acid (12[S]-HETE) and 15(S)-hydroxyeicosatetraenoic acid (15[S]-HETE). In humans, 12(S)-HETE is produced by ALOX15 and ALOX12, which are the respective products of the *ALOX15* and *ALOX12* genes (30). We have found that MCF7 cells only express *ALOX15* (Table 2), and it was shown previously that they lack *ALOX15B* (31). 12(S)-HETE was identified as a tumor cell–derived retraction factor for blood vessel endothelial cells (32). In lymphatic endothelial monolayers, 12(S)-HETE also transiently reduced VE-cadherin expression (Figure 2). These results fostered the speculation that 12(S)-HETE might be involved in MCF7-induced CCID formation.

We inhibited the enzymatic activity of ALOX15 in MCF7 cells by pharmacologic inhibition with the pan-LOX inhibitor nordihydroguaiaretic acid (33), which resulted in a significant and dose-dependent reduction of MCF7 spheroid–induced CCID areas in lymphatic endothelial cell monolayers (Supplemental Table 2). This result was confirmed with the LOX inhibitor baicalein (34) at nontoxic concentrations (Figure 3 and Supplemental Figure 6), which reduced CCID formation by 90% after 2 hours, and by 40% to 60% after 6 hours of coincubation as determined in pilot experiments (26).

Direct proof for the hypothesis that 12(S)-HETE triggered CCIDs was obtained by placing fibroblast spheroids soaked with synthetic 12(S)-HETE onto lymphatic endothelial cell monolayers. This resulted in CCID formation similar to that induced by MCF7 spheroids, whereas fibroblast spheroids imbibed with 15(S)-HETE or solvent were ineffective (Figure 3). Conversely, blocking 12(S)-HETE with a specific polyclonal antibody (35) inhibited the formation of MCF7 spheroid–induced CCIDs (Figure 3).